Magnetocrystalline anisotropy of YCo_5 and related $RECo_5$ compounds

G. H. O. Daalderop, P. J. Kelly, and M. F. H. Schuurmans
Philips Research Laboratories, Prof. Holstlaan 4, 5656 AA Eindhoven, The Netherlands
(Received 3 November 1995)

The magnetocrystalline anisotropy energy of YCo_5 has been calculated from first principles using the local-spin-density approximation. The easy magnetization axis is predicted correctly and the anisotropy energy is only 20% smaller than the experimental value if a recently proposed orbital polarization correction is included; otherwise it is about a factor of 7 too small. Our analysis indicates that magnetic materials with substantially larger anisotropy energies than the best available nowadays should be possible. A large orbital moment is found to contribute to the magnetization bringing the calculated moment, $8.0\mu_B$ per YCo_5 unit cell, into good agreement with the experimental value of $8.3\mu_B$. A large anisotropy in the magnetization is calculated which is nearly completely due to an anisotropic orbital moment associated with the Co atoms. The magnetocrystalline anisotropy energy is shown to be strongly correlated with the anisotropy in the total orbital moment. There is a large reduction in the hyperfine fields compared to the value in bulk hcp Co, not only due to large orbital contributions, but also to different values of the valence contact term. The contribution of the rare-earth (RE) ions to the anisotropy energy of the related $RECo_5$ compounds may be understood in terms of the crystal-field and exchange interactions felt by the localized RE($4f$) electrons. The RE($4f$)-Co exchange interactions and the Hartree contribution to the crystal field have been calculated under the assumption that these interactions may be treated as small perturbations. The electric-field gradient V_{zz} and the A_2^0 crystal-field parameter at the RE site are a factor of 2 and 3 larger than the experimental values, respectively. The order of magnitude of the calculated exchange field agrees with the values derived from experiment. [S0163-1829(96)01518-4]

I. INTRODUCTION

From a physical as well as from a technological point of view $RECo_5$ intermetallic compounds are of considerable interest. This is mainly due to the large magnetocrystalline anisotropy energy (MAE) of $SmCo_5$ which is about 3×10^8 ergs/cm^3 at low temperatures.[1–3] The anisotropy energy of YCo_5, which forms in the same hexagonal $CaCu_5$ structure with nearly identical lattice parameters,[4] is only a factor of 4 smaller,[5–7] and an order of magnitude larger than the anisotropy energy of bulk (hcp) cobalt[8] of 10^7 ergs/cm^3. The origin of the large magnetic anisotropy of YCo_5 compounds is not very well understood. The *difference* between the MAE of $RECo_5$ compounds and YCo_5 is found to be quite well described in terms of the interaction of the localized $4f$ electrons of a RE^{3+} ion with phenomenological crystal and exchange fields at the RE site.[1–3] The values of these fields as determined by fitting to experiment are reasonably well known but the origin of crystal fields in metallic systems and the nature of the exchange fields are not well understood quantitatively; the importance of taking into account the dependence of the exchange field on the direction of the valence electron magnetization has been pointed out by Ermolenko.[9]

The large anisotropy energy of YCo_5 has been associated with large orbital moments on the Co sites, the orbital moment on the $2c$ sites being apparently particularly large. The existence of these orbital moments was first suggested on the basis of an analysis of the magnetic form factors measured in a polarized neutron study on a YCo_5 single crystal.[10] Almost all subsequent investigations of the MAE of YCo_5 have been interpreted in the light of this neutron work. By replacing some of the Co atoms with Ni, which occupies the $2c$ site preferentially, and Fe, which preferentially occupies the $3g$ site, a correlation was established between the $2c$ site and the anisotropy energy.[6] In a study of the magnetization in high magnetic fields a (large) anisotropy in the magnetization of 4% was found.[7] From the analysis of a polarized neutron study of a $NdCo_5$ single crystal, the greater part of this magnetization anisotropy was attributed to the Co ($2c$) site;[7] in a later analysis, this anisotropy was attributed to the orbital moments on the Co sites, in particular to the Co ($2c$) site.[11]

Studies of the hyperfine field have been used to probe the site dependence of the orbital moments by relating the anisotropic component of the hyperfine field to the anisotropy in the orbital moments. Heidemann *et al.*[12] have concluded from a neutron inelastic spin-flip scattering investigation of the hyperfine fields in YCo_5 that there is (i) no significant difference in the orbital moments on the $2c$ and $3g$ sites and (ii) that there is no simple proportionality between the hyperfine fields and the Co moments. Nuclear magnetic resonance (NMR) measurements of the hyperfine field have also been carried out.[13–15] Under the assumption that the orbital moment *is* proportional to the orbital hyperfine field, it was concluded from these studies that the large magnetic anisotropy of YCo_5 is related to a large orbital moment on the $2c$ site.

Most of the information about the crystal fields and exchange fields in the $RECo_5$ compounds has been obtained indirectly by treating these interactions as free parameters in crystal-field calculations of the MAE and varying them so as to obtain reasonable agreement with the temperature dependence of the single-ion contribution to the MAE as determined experimentally. Values for the crystal-field parameter

$A_2^0\langle r^2\rangle/k_B$ of -180,[1] -420,[2] and -185 K,[3] and for the exchange-field parameter $\mu_B B_{EX}/k_B$ of 200,[1] 240,[2] and 100 K (Ref. 3) have been reported for $SmCo_5$. Studies of the hard-axis magnetization curves have been used to determine the exchange field acting on the RE ions. For $Y_{1-x}Gd_xCo_5$ alloys a value of the exchange field of 150 K was found.[9] ^{155}Gd Mössbauer spectroscopy studies have allowed a determination of the electric-field gradients on the Gd site in $GdCo_5$;[16, 17] in a simple crystal-field picture based on ionic charges, the electric-field gradient at the nucleus is simply related to the crystal field seen by the $4f$ electrons.

Independent information and insight can be obtained from *ab initio* calculations based on the Hohenberg-Kohn-Sham density-functional formalism.[18,19] Within the framework of the local-spin-density approximation[20,21] (LSDA) to the density-functional formalism, ground-state properties may be calculated without use of any free parameters; the only inputs are the crystal structure and lattice parameters. In this paper we will concentrate on the magnetic properties of YCo_5; in particular we will be interested to see whether the relatively large magnetocrystalline anisotropy energy of this compound can be calculated within the LSDA. In an earlier study of the MAE of Fe, Co, and Ni,[22] we found that although the correct order of magnitude of the anisotropy energy could be calculated, the incorrect sign was obtained for Co and Ni. For Co the calculation was in error by 0.08 meV. Since the MAE per Co atom in YCo_5 is ~ 0.76 meV or almost an order of magnitude larger, an absolute error of 0.08 meV per Co atom would be a very acceptable result. We shall see that this is not the case. The straightforward LSDA calculation results in a MAE of 0.54 meV per unit cell which is about a factor of 7 too small and represents an error of 0.65 meV per Co atom. In addition, we find that the magnetization is also significantly underestimated. The orbital moment contribution to the magnetization is apparently too small, just as we found for Co. If a recently proposed orbital polarization term,[23–25] whose main effect is to enhance the orbital moment, is included, then a magnetization of $8.0\mu_B$ per unit cell is obtained compared to the experimental value[7] of $8.3\mu_B$. The corresponding anisotropy energy of 3.0 meV per unit cell is in acceptable agreement with the experimental value of 3.8 meV per unit cell. We find a strong correlation between the anisotropy energy and the average anisotropy in the orbital moment per Co atom.[26] At the actual Fermi energy the orbital anisotropy on the $3g$ site is larger than that on the $2c$ site. No significant difference between the orbital moments on the $2c$ and $3g$ sites is found. In order to try and understand the discrepancy between this result and the picture derived from neutron scattering[10] and confirmed by NMR,[13–15] we calculated the hyperfine fields. It appears, however, that the hyperfine fields cannot be calculated with sufficient accuracy[27] to allow the NMR experiments to be reinterpreted with confidence.

If we assume that the crystal-field and exchange interaction between the RE $4f$ electrons and the other valence electrons is sufficiently weak that it may be treated as a small perturbation, then these parameters can be evaluated from first principles. The calculated second-order crystal-field parameter[28] and the electric-field gradient are about a factor of 2–3 larger than the values extracted from experiment. The calculated exchange field agrees with the experimental values. Brief summaries of the results of the YCo_5 anisotropy-energy and crystal-field calculations $GdCo_5$ have been given in Refs. 26 and 28, respectively.

The paper is organized as follows. The theoretical methods used are described in Sec. II. In Sec. III the results of our calculations are described and compared with experimental results and other calculations. A brief summary with some conclusions is given in Sec. IV.

II. METHOD

Within the density-functional formalism,[18] Kohn and Sham showed[19] that the many-electron problem for the ground state of an inhomogeneous interacting electron gas in an external potential may be reduced to an effective independent particle problem, the Kohn-Sham equations[19] which must be solved self-consistently, usually by iteration. In practical calculations explicit expressions for the exchange-correlation energy and potential are required and the usual approach is to make the local-spin-density-approximation.[20,21] In this work we have used two different methods to solve the Kohn-Sham equations. A full potential (FLAPW) version[29] of the linear-augmented plane-wave (LAPW) method[30] is used for calculations of the electric-field gradient, crystal-field parameters and contact contributions to the hyperfine field. In a so-called full potential method, there is no restriction imposed on the form of the potential or spin density; these are not assumed to be spherically symmetrical inside atom-centered spheres as in the muffin tin (MT) or atomic sphere (AS) approximations. By performing convergence tests on the number of plane waves in the basis, on the upper angular momentum used in the expansion of the potential around the atom sites and the spherical harmonic expansion of the plane waves inside a MT sphere, on the number of **k** points[31] used to sample the Brillouin zone (BZ) and on the number of fixed energies around which the energy linearization is performed, essentially exact solutions of the Kohn-Sham equations within the LSDA can be obtained. To obtain reliable results for the magnetization and the energy bands of YCo_5, we found that about 70 plane waves/atom were required so that matrices of rank 400 had to be diagonalized.

For calculations of the MAE a fine sampling of the Brillouin zone must be made and calculations with the FLAPW method would be very time consuming. In order to calculate the MAE, orbital moments, orbital contributions to the hyperfine field and local exchange interactions between RE $4f$ magnetic moments and the valence electron magnetization we use the efficient linear muffin-tin orbital (LMTO) method in the atomic-sphere approximation (ASA).[30] In LMTO calculations a basis of typically 16 (s, p, d, and f) orbitals per atom is used making the LMTO method about two orders of magnitude faster than the FLAPW if the matrix diagonalization is the most computationally demanding step. If the ASA, in which the potential is assumed to have spherical symmetry inside atomic spheres which replace the atomic Wigner-Seitz cell, is used then this is the case.

In Sec. II A we describe the approximations used to calculate the magnetocrystalline anisotropy energy of the itinerant valence electrons. In Sec. II B expressions for contact and orbital contributions to the hyperfine field are given. The

calculation of crystal-field parameters as well as the electric-field gradient is described in Sec. II C. In Sec. II E the approximations used to calculate local exchange interactions between the RE spin and the valence electron magnetization are discussed. Some specific technical details of the LMTO and FLAPW calculations are given in Sec. II F.

A. Itinerant electron anisotropy energy

Magnetocrystalline anisotropy refers to the dependence of the ground-state energy on the orientation of the magnetization and, microscopically, it occurs when both exchange-splitting and spin-orbit coupling are included in the Hamiltonian. In $3d$ transition-metal systems the spin-orbit coupling parameter of the valence electrons is much smaller than the exchange-splitting and the bandwidth. One can therefore make the approximation of first solving the Kohn-Sham equations for the scalar-relativistic spin-polarized Hamiltonian self-consistently and of including the spin-orbit coupling in a subsequent non-self-consistent step.[32] The Kohn-Sham eigenvalues then obtained by diagonalization of the Hamiltonian depend on the direction $\mathbf{n}$ of the magnetization. The change in total energy upon inclusion of the spin-orbit coupling, as given by the change in the single-particle eigenvalue sum, is correct to first order in the changes in the electron and spin densities occurring upon a rotation of the magnetization direction.[22] The MAE due to the valence electrons is then approximately[22]

$$\Delta E=\Delta E^n(\mathbf{n}_1,\mathbf{n}_2)=\Delta E(n,\mathbf{n}_1)-\Delta E(n,\mathbf{n}_2)$$
$$\approx\sum_{i,\mathbf{k}}^{\text{occ}}\varepsilon_i(\mathbf{k},\mathbf{n}_1)-\sum_{i,\mathbf{k}}^{\text{occ}}\varepsilon_i(\mathbf{k},\mathbf{n}_2)=\int_{\text{BZ}}d\mathbf{k}\Delta\mathscr{E}^n(\mathbf{k}). \quad (1)$$

where n is the number of valence electrons. The band index i must be summed over all occupied states up to the Fermi energy $\varepsilon_F^n(\mathbf{n}_{\boldsymbol{\alpha}})$ and the $\mathbf{k}$ summation is over the first Brillouin zone. $\Delta\mathscr{E}^n(\mathbf{k})$ is the anisotropy energy density in $\mathbf{k}$ space. At this point it will be convenient to choose the directions $\mathbf{n_1}$ and $\mathbf{n_2}$ to be the x (the anisotropy in the basal plane is known to be small and can be neglected) and z directions, respectively, and the explicit dependence of the anisotropy energy on the two magnetization directions will be suppressed from now on. As in our earlier work,[26, 33] the eigenvalue sums were evaluated directly with the improved tetrahedron method[31] without having to use the density-of-states or number-of-states functions.[22]

To investigate how the anisotropy energy depends on the location of the Fermi energy, we calculate the difference of two single-particle eigenvalue sums as a function of the non-integer band filling q using the band structure calculated self-consistently for n electrons. We call this quantity $\Delta E^n(q)$. By plotting the corresponding generalized anisotropy energy density $\Delta\mathscr{E}^n(\mathbf{k},q)$ in the BZ as a function of the band filling q we can identify the contribution of particular states $|i\mathbf{k}\rangle$ to the anisotropy energy. The dependence of the Fermi energy on the number of valence electrons n and the magnetization direction $\mathbf{n}$ will not be shown explicitly in the following.

Atom projected orbital angular momenta oriented along $\mathbf{n}$ are calculated using

TABLE I. $\delta E(n,L_{\max},S)$, the difference in energy between the lowest term in a given d^n configuration with maximum spin S and the L averaged energy of that configuration in units of the Racah B parameter. Results from atomic theory are compared with a simple interpolation formula $-L^2/2$.

	d^1	d^2	d^3	d^4
Racah	0	$-\frac{9}{2}$	$-\frac{9}{2}$	0
$-L^2/2$	-2	$-\frac{9}{2}$	$-\frac{9}{2}$	-2

$$L(\tau)=\sum_{i,\mathbf{k}}^{\text{occ}}\langle\psi_{i,\mathbf{k}}^{\mathbf{n}}|\mathbf{n}\cdot\boldsymbol{l}|\psi_{i,\mathbf{k}}^{\mathbf{n}}\rangle_{\text{AS}}, \quad (2)$$

where $\psi_{i,\mathbf{k}}^{\mathbf{n}}$ is the eigenstate of energy band i with wave vector $\mathbf{k}$ calculated for the magnetization direction $\mathbf{n}$ and the subscript AS indicates that the integral is performed over the atomic sphere of the atom τ in question.

The orbital moments obtained from LSDA calculations for Fe and Co (but not for Ni) are about a factor of 2 smaller than the experimental values.[22, 25] Recently it was shown that inclusion of a term proportional to $2L\mathbf{n}\cdot\boldsymbol{l}$ in the Kohn-Sham equations improved the calculated properties of certain $4f$ and $5f$ systems considerably,[24] and led to enhanced orbital moments in Fe, Co, and Ni.[25] This so-called orbital polarization term (OP) is based upon an approximate L^2 dependence of the energy of the lowest term of a given configuration with respect to the average energy of all terms of the same configuration with maximum spin for an *atom*. This dependence is assumed to be transferred to the solid state.

For an atom obeying Russell-Saunders coupling, a d^n or f^n electronic configuration with maximum spin S will split into terms with different values of the total orbital angular momentum L. The term with the largest $L(=L_{\max})$ is lowest in energy (Hund's rules). The energy difference between this term with $L=L_{\max}$ and the weighted average of the terms with maximum spin is[34]

$$\delta E(n,L_{\max},S)=E(n,L_{\max},S)-\overline{E}$$
$$=E(n,L_{\max},S)-\frac{\Sigma_L(2L+1)E(n,L,S)}{\Sigma_L(2L+1)}. \quad (3)$$

This energy is given in Tables I and II for d^n or f^n configurations, respectively. The contention of Brooks *et al.* is that the L dependence of $\delta E(n,L,S)$ can be interpolated approximately by $-(B/2)L^2$, respectively $-(E^3/2)L^2$, if n is varied in d^n or f^n configurations with maximum spin multiplicity.

TABLE II. $\delta E(n,L_{\max},S)$, the difference in energy between the lowest term in a given f^n configuration with maximum spin S and the L averaged energy of that configuration in units of the Racah E^3 parameter. Results from atomic theory are compared with a simple interpolation formula $-L^2/2$.

	f^1	f^2	f^3	f^4	f^5	f^6
Racah	0	-9	-21	-21	-9	0
$-L^2/2$	$-\frac{9}{2}$	$-\frac{25}{2}$	-18	-18	$-\frac{25}{2}$	$-\frac{9}{2}$

The simple interpolation formula tends to overbind terms with nearly empty or nearly filled shells. B and E^3 are Racah parameters.[34] B is given by

$$B=\frac{9F^2-5F^4}{441}, \tag{4}$$

where the Slater F^k integrals are given by

$$F^k=\int\int \phi_d^2(r_1)\phi_d^2(r_2)\frac{2r_<^k}{r_>^{k+1}}r_1^2r_2^2dr_1dr_2. \tag{5}$$

in terms of integrals involving the radial d wave function ϕ_d. For a crystal we replace ϕ_d with the d partial wave evaluated at the center of gravity of the occupied part of the d band, $\phi_d(\overline{\varepsilon},r)$.

We have investigated the influence of orbital polarization on the calculated orbital moments and the MAE by including a term $-BL\mathbf{n}\cdot\boldsymbol{l}$ in the Hamiltonian and iterating to self-consistency with the magnetization direction parallel to the c axis. This yields new self-consistent orbital angular momenta, orbital splittings BL and a new self-consistent potential. It can be shown that upon a rotation of the magnetization direction, the change in total energy is given by the change in the one-particle sum correct to first order in the changes in the electron and spin densities and in the orbital angular momentum.[35] Using the self-consistently determined orbital splittings the anisotropy energy may be calculated as previously [Eq. (1)], using the new self-consistent potential calculated including OP.

Classical magnetic dipolar interactions between magnetic moments are another source of anisotropy energy, not included in the theory described above. The interatomic magnetostatic energy, $E^{\mathrm{dip-dip}}$, is given by

$$E^{\mathrm{dip-dip}}=\frac{1}{c^2}{\sum_{\mathbf{R},\tau,\tau'}}'\frac{1}{|\mathbf{R}+\tau-\tau'|^3}\left(\mathbf{m}_\tau\cdot\mathbf{m}_{\tau'}-3\frac{[(\mathbf{R}+\tau-\tau')\cdot\mathbf{m}_\tau][(\mathbf{R}+\tau-\tau')\cdot\mathbf{m}_{\tau'}]}{|\mathbf{R}+\tau-\tau'|^2}\right), \tag{6}$$

where $\mathbf{m}_\tau$ is the total magnetic moment in an atomic sphere centered on site τ. After the shape anisotropy has been excluded,[22] $E^{\mathrm{dip-dip}}$ can be determined for different orientations of the magnetic moments.

B. Hyperfine fields

The hyperfine field B_{hf} at a nucleus comprises a Fermi contact interaction term,[36] an orbital hyperfine field and dipolar contributions. The latter are of order 1 T and are generally neglected. The Fermi contact interaction is determined by the magnetization density at the nucleus, while the orbital hyperfine field is related to the orbital moment of the valence electrons only; contributions from core electrons have been shown to be negligible ($\sim$0.1 T).[37] If it is assumed that the contact and orbital hyperfine interactions are proportional to the spin and orbital moments, respectively, then measurements of the hyperfine fields can be used to obtain information about the site dependence of the magnetization.

In our calculation of the hyperfine field B_{hf}, we follow the treatment of Blügel *et al.* who derived expressions for the orbital, dipolar, and contact contributions to the hyperfine fields, which should be used in conjunction with scalar relativistic wave functions.[38] Because of the divergence of the (scalar) relativistic s wave functions at the nucleus, the relativistic generalization of the Fermi contact hyperfine field (in SI units),

$$B_c=\frac{8\pi}{3}\frac{\mu_0}{4\pi}m(0), \tag{7}$$

where $m(0)$ is the magnetization density at the nucleus, is

$$B_c=\frac{8\pi}{3}\frac{\mu_0}{4\pi}m_{\mathrm{av}}, \tag{8}$$

where m_{av} is an averaged magnetization density given by $m_{av}=\int d\mathbf{r}\delta_T(\mathbf{r})m(\mathbf{r})$ and $m(\mathbf{r})$ is the magnetization density due to s electrons. $\delta_T(\mathbf{r})$ is essentially a smeared out δ function, $\delta_T(\mathbf{r})=(1/4\pi r^2)(\partial S/\partial r)$, where $S(\mathbf{r})$ is the reciprocal of the relativistic mass enhancement $S^{-1}(\mathbf{r})=1+[\varepsilon-V(\mathbf{r})]/2mc^2$. The most important contribution to B_c is obtained for r values smaller than or of order of the Thompson radius $r_T=Ze^2/mc^2$. Adapting Eq. (7) to the relativistic case by simply averaging the relativistic wave functions over the nuclear volume leads to overestimates of the contact hyperfine field.

Similarly, the orbital contribution to the hyperfine field is given by[38]

$$B_{\mathrm{orb}}=\frac{2\mu_0\mu_B}{4\pi}L_{\mathrm{av}}, \tag{9}$$

with

$$L_{\mathrm{av}}=\sum_{i,\mathbf{k}}^{\mathrm{occ}}\langle\psi_{i,\mathbf{k}}^{\mathbf{n}}|\frac{S(r)}{r^3}\mathbf{n}\cdot\boldsymbol{l}|\psi_{i,\mathbf{k}}^{\mathbf{n}}\rangle_{\mathrm{AS}}. \tag{10}$$

C. Crystal-field parameters

Most RE atoms in a solid may be regarded as being in an $f^{n-3}(sd)^3$ or trivalent electronic configuration, which is well separated from other configurations [such as $f^{n-2}(sd)^2$ or $f^{n-4}(sd)^4$] by $\sim$5 eV. Within this trivalent configuration the term with the lowest energy is obtained by first maximizing the spin S and then maximizing the orbital angular momentum L; the $4f$ electrons approximately obey Russell-Saunders (LS) coupling.[39] Spin-orbit coupling splits each term into multiplets ${}^{2S+1}L_J$, where the total angular momentum J of the ground-state multiplet is given by $J=|L-S|$ or $J=|L+S|$ for less-than or more-than half filled $4f$ shells, respectively. When the RE atom is embedded in a crystal, the $(2J+1)$-fold degenerate ground state will split according to the irreducible representations of the point-group. Because of the localization, and the (related) large intra-atomic electron-electron interactions of the $4f$ electrons of the RE atoms, the lowering of the point-group symmetry from spherical symmetry due to the crystalline environment usually represents a weak perturbation to the ground state of a RE atom in a solid.

The potential describing these crystal-field effects (felt by each f electron) can be expanded around the RE site (we omit the explicit site index) into radial and angular parts

$$v(\mathbf{r})=\sum_{l\alpha} v_{l\alpha}(r)K_{l\alpha}(\hat{r}), \tag{11}$$

where $l\alpha$ labels the real lattice-harmonics $K_{l\alpha}$ which have been symmetrized according to the local point-group symmetry. In order to make contact with previously published work we write the lattice harmonics in terms of the functions $f_{lm}(\mathbf{r})$ used by Hutchings[40]

$$K_{l\alpha}(\hat{r})=\sum_{l,m} c^{\alpha}_{lm}\frac{f_{lm}(\mathbf{r})}{r^l}. \tag{12}$$

For example, $f_{20}(\mathbf{r})=3z^2-r^2$. If all $4f$ one-electron states have the same radial dependence $\phi_{4f}(r)$, the matrix elements of the Hamiltonian between states of the ground-state multiplet $|LSJ,M=M_J\rangle$ can be written

$$\mathscr{H}^{\mathrm{CF}}_{MM'}=\langle LSJM|(-e)\sum_i v(\mathbf{r}_i)|LSJM'\rangle$$

$$=\sum_{l,m} A^m_l\langle r^l\rangle\theta^{LSJ}_l\langle JM|O^m_l|JM'\rangle, \tag{13}$$

as a consequence of the Wigner-Eckart theorem,[41] with

$$A^m_l\langle r^l\rangle=(-e)\sum_{\alpha}\int \phi^2_{4f}(r)c^{\alpha}_{lm}v_{l\alpha}(r)r^2dr. \tag{14}$$

The crystal-field parameters are thus determined by the radial dependence of the potential $v_{l\alpha}(r)$ and the $4f$ radial wavefunction $\phi_{4f}(r)$. θ^{LSJ}_l is the ratio between two reduced matrix elements in the Wigner-Eckart theorem. If the O^m_l are chosen as Stevens operator equivalents[42,40] to f_{lm} for the ground state $|LSJ\rangle$ then $\theta^{LSJ}_l=\alpha_J,\beta_J,\gamma_J$ for $l=2$, 4, and 6, respectively. These have been tabulated in Refs. 42 and 40. As the crystal-field splitting is in general much smaller than the splitting between multiplets, one usually neglects the mixing-in of excited multiplets with different values of J in the Hamiltonian, as in Eq. (13). For f states, the number of crystal-field parameters A^m_l is limited to $l\leqslant 6$ and l even. The local point-group symmetry determines the coefficients c^{α}_{lm}, and this further restricts the number of independent parameters A^m_l for each value of l. For the RE atom in $RECo_5$, the local point-group symmetry is D_{6h}, leading to independent parameters A^m_l with $(l,m)=(2,0)$; (4,0); (6,0) and (6,6).

The simplest approximation to the one-electron potential $v(\mathbf{r})$ is the electrostatic (Coulomb) part of the potential generated by the self-consistent charge density in the crystal. Within a muffin-tin sphere around the RE site it can be expressed as[43]

$$v(\mathbf{r})=\sum_{l\alpha} v_{l\alpha}(r)K_{l\alpha}(\hat{r})=\sum_{l\alpha}\frac{4\pi}{2l+1}[U_{l\alpha}(r)+r^l\tilde{q}_{l\alpha}]K_{l\alpha}(\hat{r}), \tag{15}$$

where $v_{l\alpha}(r)$ is divided into on-site and lattice contributions. The on-site contribution is

$$\frac{4\pi}{2l+1}U_{l\alpha}(r)=\frac{4\pi}{2l+1}\int_o^R\frac{r^l_<}{r^{l+1}_>}\rho_{l\alpha}(r')r'^2dr', \tag{16}$$

where $\rho_{l\alpha}(r)$ follows from an expansion of the charge density around the RE atom and R is the radius of the muffin-tin sphere centered on the RE site

$$\rho(\mathbf{r})=\sum_{l\alpha}\rho_{l\alpha}(r)K_{l\alpha}(\hat{r}). \tag{17}$$

The lattice contribution which depends on the charge density outside the muffin-tin sphere, and on the requirement of continuity of the potential[43] is more complicated and will not be given explicitly here. We note that while splitting the potential into an on-site and a lattice contribution does not involve any approximation, for a continuous charge distribution it does require a somewhat arbitrary partitioning of the charge density as determined by the choice of the muffin-tin radius R.

The on-site nonspherical potential generated by the $4f$ charge density, $v^{4f}_{l\alpha}$, should be excluded from $v_{l\alpha}$ in Eq. (14). It corresponds to a self-energy of the $4f$ charge density that by itself does not give rise to a crystal-field splitting. We have spherically averaged the $4f$ charge density, treating the $4f$ states as core states but allowing the radial distribution to adjust to changes in the valence charge density. The nonspherical $4f$ charge density would influence the valence electron charge density but we have not investigated this further. $v(\mathbf{r})$ is calculated self-consistently using the FLAPW method.

The anisotropy energy is the difference between the ground-state energies corresponding to the two directions of magnetization $\hat{x}$ and $\hat{z}$. On rotating the magnetization direction, the valence electron charge density and potential are assumed not to change and thus the crystal-field parameters, defined with respect to the crystal axes are unchanged. In the large exchange limit,[3] the ground state has a maximal azimuthal quantum number $M=J$ directed along the magnetization direction. The single ion anisotropy is then given by

$$A^0_2\langle r^2\rangle\alpha_J\langle J,M=J|3J^2_z-3J^2_x|J,M=J\rangle$$

$$=A^0_2\langle r^2\rangle\alpha_J\frac{3}{2}(2J^2-J). \tag{18}$$

D. Electric-field gradient

The electric-field gradient (EFG) at the RE nucleus is given by[44]

$$V_{zz}=\left(\frac{\partial^2}{\partial z^2}-\frac{1}{3}\nabla^2\right)v(\mathbf{r})\Big|_{r=0}$$

$$=\frac{\partial^2}{\partial z^2}(r^2K_{20}(\hat{r}))\lim_{r\to 0}\frac{v_{20}(r)}{r^2}$$

$$=4c_{20}\lim_{r\to 0}\frac{v_{20}(r)}{r^2}=\sqrt{\frac{5}{\pi}}\lim_{r\to 0}\frac{v_{20}(r)}{r^2}, \tag{19}$$

where again the site index has been omitted for simplicity. If the $4f$ charge-density were located at the nucleus $r\to 0$, or if

$v_{20}(r)/r^2$ were independent of r, then A_2^0 would be equal to $-(e/4)V_{zz}$. This follows from Eqs. (14) and (19). A different proportionality than $-e/4$ is therefore entirely due to the on-site contribution of the potential; any deviation being caused by the overlap between the $4f$ corelike charge density and the nonspherical on-site valence charge density.

E. Exchange interaction

So far the valence electron MAE and single ion anisotropy have been treated separately. However, the directions of the localized RE moment and the valence electron magnetization are correlated. This exchange coupling, together with the crystal-field parameters and the MAE of the valence band electrons, determines to what extent the RE $4f$ and Co $3d$ magnetic moments are aligned. Phenomenologically, it is taken into account in the RE Hamiltonian by an exchange field $\mathbf{B}_{\mathrm{EX}}$ coupling to the $4f$ spin[1–3,9]

$$\mathscr{H}_{\mathrm{EX}}=2\mu_B\mathbf{S}\cdot\mathbf{B}_{\mathrm{EX}}. \tag{20}$$

If the $4f$ electrons do not hybridize with the valence electrons, this Hamiltonian must express the dependence of the energy of $4f$ spins in a spin-polarized potential, supplied by the spin polarized valence electrons. This is similar to the contribution to the exchange energy of a free atom from coupling between open shells.[45] Within the LSDA the exchange energy can be expressed in terms of local exchange integrals. The exchange energy which the $4f$ electrons gain if placed in a spin-polarized potential generated by the valence electrons is

$$\Delta E_{\mathrm{EX}}=n^{\uparrow}\varepsilon^{\uparrow}+n^{\downarrow}\varepsilon^{\downarrow}-(n^{\uparrow}+n^{\downarrow})\frac{\varepsilon^{\uparrow}+\varepsilon^{\downarrow}}{2}, \tag{21}$$

where n^{σ} is the number of $4f$ electrons with spin σ and one particle energy ε^{σ}. The difference in the single-particle energies is given by

$$\varepsilon^{\uparrow}-\varepsilon^{\downarrow}=\int \phi_{4f}^2(r)[v_{\uparrow}(r)-v_{\downarrow}(r)]r^2dr \tag{22}$$

in terms of the spin-dependent potential on the RE site. The parametrization of the exchange correlation potential used in the rest of this work,[20] may be further approximated:

$$\begin{aligned} v_{\uparrow}(r)-v_{\downarrow}(r)&\cong\frac{2}{3}A(r_s)\frac{\rho_{\uparrow}(r)-\rho_{\downarrow}(r)}{\rho(r)}\\ &\cong\sum_l\frac{2}{3}A(r_s)\frac{\Delta n_l}{4\pi}\frac{\phi_l^2(\varepsilon_F,r)}{\rho(r)}, \end{aligned} \tag{23}$$

where $A(r_s)$ is a known function of the density[20] and Δn_l is the difference in the number of spin-up and spin-down valence electrons with angular momentum character l. $\phi_l(\varepsilon_F,r)$ is the partial wave with angular momentum character l and energy ε_F. Thus the simple result is obtained that[46]

$$\Delta E_{\mathrm{EX}}=-\frac{1}{2}\sum_l \Delta n_l I_{l,4f}\Delta n_{4f}, \tag{24}$$

where $I_{l,l'}>0$ is the local exchange-integral matrix:

$$I_{l,l'}=-\frac{2}{3}\int \phi_l^2(r)\phi_{l'}^2(\varepsilon_F,r)\frac{A(r_s)}{4\pi\rho(r)}r^2dr. \tag{25}$$

A comparison with the phenomenological exchange Hamiltonian, Eq. (20), shows that

$$\mu_B B_{\mathrm{EX}}=-\frac{1}{2}\sum_l \Delta n_l I_{l,4f}. \tag{26}$$

The $4f$ spins interact with the on-site valence electron magnetization through local exchange interactions $I_{l,4f}$. The on-site valence electron magnetization is caused by the hybridization of the RE $5d$ electrons with the Co $3d$ electrons.[46] The high-lying $5d$ bands hybridize more strongly with minority Co $3d$ bands than with majority $3d$ bands, due to the large exchange splitting of the Co $3d$ bands. Thus the magnetic moment derived from RE $5d$ valence electrons is directed antiparallel to the overall valence electron magnetization. Together with the local ferromagnetic exchange interaction $I_{l,4f}$ the direction of the total localized RE magnetic moment now depends on whether the $4f$ shell is more than or less than half filled, and on the magnitude of L compared to S.

It has been pointed out by Liebs, Hummler, and Fähnle[47] that the perturbative approach sketched above can be improved upon by performing two separate self-consistent field calculations with the $4f$ moments rotated by 180° and evaluating the change in the total energy. In this way the conduction electron spins are allowed to adjust to the reversed exchange field; this turns out to be an important quantitative effect.

F. Details of the calculation

The $CaCu_5$ structure (space group No. 191) has hexagonal symmetry (point-group $P6/mmm$). Inequivalent Cu atoms occupy the $2c$ and $3g$ Wyckoff sites. For YCo_5 the lattice parameters used are $a=9.313$ a.u. and $c=7.544$ a.u.[4] For $GdCo_5$ the lattice parameters are $a=9.398$ a.u. and $c=7.500$ a.u.[4] The von Barth-Hedin parametrization of the exchange-correlation potential is used.[20] The Brillouin-zone integration is performed using the improved tetrahedron method.[31]

The LMTO basis states are the nearly orthogonal Θ functions devised by Andersen and Jepsen.[48] s, p, d, and f partial waves are included in the basis. Self-consistent charge densities are obtained using 2366 **k** points in the full Brillouin zone, corresponding to 133 inequivalent **k** points. The calculated atom-projected magnetic moments change by about $0.002\mu_B$ if 3600 **k** points (196 inequivalent **k** points) are used. Atomic sphere radii of Y and Co are 3.497 and 2.645 a.u., respectively, leading to a maximum overlap of about 14.2%, which is comparable to the overlap in a bcc lattice.

In the FLAPW calculations the nonoverlapping Y and Co muffin-tin radii were 3.10 and 2.31 a.u., respectively. A plane-wave cutoff of $K_{\max}=3.5$ a.u. was used, so that the basis contained about 415 plane waves or 70 plane waves per atom. In the second-variation step where the nonspherical terms in the potential are treated, an energy cutoff of $\varepsilon_{\max}=3.5$ Ry was used, corresponding to about 85 basis

TABLE III. Calculated magnetic moments of YCo_5 within the muffin-tin and atomic spheres using the FLAPW (column 2) and LMTO methods (columns 3–7), respectively. The spin and orbital moments in columns 4 and 5 result from including spin-orbit coupling non-self-consistently. The spin and orbital moments in columns 6 and 7 were calculated self-consistently including spin-orbit coupling and orbital polarization. Experimental values for the total magnetic moment are 8.33 (Ref. 7) and 8.13 (Ref. 5) μ_B at 4.2 K, and 8.0 (Ref. 7) and 7.99 (Ref. 10) μ_B at room temperature.

	FLAPW	LMTO				
			SO		SO+OP	
	σ	σ	σ	l	σ	l
Y	-0.27	-0.31	-0.31	0.02	-0.32	0.04
Co($2c$)	1.46	1.32	1.32	0.12	1.33	0.23
Co($3g$)	1.51	1.49	1.49	0.12	1.51	0.23
Interst.	-0.28					
Total	6.90	6.78	6.78	0.61	6.84	1.20

states. Checks with $K_{\max}=3.0$ a.u. (275 basis functions) and $\varepsilon_{\max}=3.0$ Ry were performed, yielding $\leqslant 0.05\mu_B$ changes in the total magnetic moment, and 10% changes in crystal-field parameters. Reciprocal space integrations were carried out with 1100 **k** points in the full Brillouin zone (72 inequivalent **k** points). The total magnetic moment is then converged to within $0.02\mu_B$.

III. RESULTS AND DISCUSSION

Before describing the magnetocrystalline anisotropy energy of YCo_5 in Sec. III C, the calculations of the magnetization and hyperfine fields are presented in Sec. III A and Sec. III B, respectively. The results of the calculations of the crystal-field parameters, the electric-field gradient and the exchange field are discussed in Sec. III D.

A. Magnetization

The magnetic moment per unit cell as measured by several groups of workers[10,5,7] on single crystals of YCo_5 is given in Table III together with the spin contribution to the magnetic moment calculated using the LMTO and FLAPW methods. The single-crystal measurements are in fair agreement with each other, values ranging between 8.0 and $8.4\mu_B$ per unit cell. Measurements on powder samples tend to result in values for the magnetization which are about 1 μ_B lower than the single-crystal data. A considerably lower spin magnetic moment of 6.8 and $6.9\mu_B$ per unit cell is calculated using the LMTO and FLAPW methods, respectively. The discrepancy per Co atom with the experimental value is much larger than the difference found for the transition metal elements Fe, Co, and Ni. A possible reason for this discrepancy is the neglect of orbital contributions to the magnetization. Including spin-orbit coupling (non-self-consistently) in the Hamiltonian, a large orbital moment of $0.6\mu_B$ per unit cell is found, whereby each Co atom contributes on average $0.12\mu_B$. This is about 50% more than the orbital moment of $0.08\mu_B$ calculated in the same way for hcp Co. The spin magnetic moment is not changed significantly by including spin-orbit coupling so that a fairly large discrepancy with the experimental magnetic moment remains.

Inclusion of orbital polarization in local-spin-density calculations leads to increased orbital moments and considerably better agreement with experiment for several systems.[24,25] For example, for hcp Co the calculated orbital moment is then $0.13\mu_B$,[26,49] compared to the experimental value of $0.16\mu_B$, and the total magnetic moment is $1.70\mu_B$, compared with the experimental value of $1.75\mu_B$. Including both OP and SO interactions in the YCo_5 calculation, and iterating to self-consistency, a total orbital moment of $1.2\mu_B$ is calculated, yielding a total magnetic moment of $8.0\mu_B$ per unit cell. This value is in good agreement with the experimental values for single crystals. The discrepancy between the calculated and experimental magnetic moment per Co atom is approximately equal to the discrepancy found for hcp Co.

We thus find a very large orbital moment of $0.23\mu_B$ on each Co atom. Magnetic form factor measurements by means of neutron-scattering experiments[10] had already indicated the existence of large orbital moments. However, it was concluded from an analysis of these measurements that the orbital moment at the $2c$ site ($0.46\mu_B$) is nearly twice that at the $3g$ site ($0.28\mu_B$). In addition, it was found that the spin magnetization density around the $2c$ site extends in the basal plane, and deviates strongly from spherical symmetry. Our calculations do not support these two conclusions. We find *equal* orbital moments for each Co site and we find for $GdCo_5$ and YCo_5 using the FLAPW method that the deviation from a relative occupation of 0.2 for each d orbital within the muffin-tin sphere is $\leqslant$ 0.01 at the $2c$ sites. However at the $3g$ sites the deviation may amount to as much as 0.04 (i.e., 20%) for some of the d orbitals. The spin density within the muffin-tin spheres is not found to contain such large deviations from spherical symmetry as was deduced from the form factor measurements.

Comparison with previous work

In an early self-consistent spin-polarized augmented plane-wave calculation[50] based on Slater's $X\alpha$ approximation with $\alpha=1$ (which is known to overestimate the tendency to ferromagnetic ordering), a total spin magnetic moment of $7.31\mu_B$ per unit cell was found for YCo_5. In this calculation, the two inequivalent Co sites were considered to be equivalent.

A self-consistent LMTO calculation by Szpunar and Smith[51] yielded a spin magnetic moment of $m_{\rm tot}=m_{\rm Y}+m_{{\rm Co}(2c)}\times 2+m_{{\rm Co}(3g)}\times 3=-0.37+1.29\times 2+1.44\times 3=6.54\mu_B$ per unit cell. The negative moment on the Y site is larger than the value which we found. This is probably attributable to Szpunar and Smith's use of an atomic sphere which was 9% larger in volume than the atomic sphere which we used and to the interstitial spin density being negative in sign (as found, for example, in our FLAPW calculation; see Table III).

In another self-consistent LMTO calculation, Nordström *et al.*[52] found a total spin magnetic moment per unit cell of $-0.27+1.44\times 2+1.37\times 3=6.72\mu_B$ which is in good agreement with the value which we found. Curiously, these authors find that the moment on the $2c$ site is larger than the

TABLE IV. Measured and calculated hyperfine fields in Tesla for Fe, Co, and Ni and at the Co ($2c$) and ($3g$) sites in YCo_5 and $GdCo_5$. Core, valence, and orbital contributions to the hyperfine fields are listed separately. The orbital hyperfine fields, as well as the total hyperfine fields are calculated using spin-orbit coupling only (listed in the columns denoted by SO), as well as using spin-orbit coupling and orbital polarization (listed in the columns denoted by OP). Various experimental results are shown in the last column.

	Core	Val	Orb		Total		Expt.
			SO	OP	SO	OP	
Fe	-25.3	-4.3	+3.5	+5.5	-26.1	-24.1	-33.9
Co	-18.9	-7.2	+4.5	+8.0	-21.6	-18.1	-21.5
Ni	-7.5	-2.8	+5.5	+8.0	-4.8	-2.3	-7.5
$YCo_5(2c)$	-16.8	+5.0	+8.3	+16.4	-3.5	+4.6	-8.7[a]
							-9.9[b]
							-9.5[c]
							+1.5[d]
$YCo_5(3g)$	-17.3	-5.2	+8.9	+18.3	-13.6	-4.2	-14.1[a]
							-13.9[b]
							-9.5[c]
							-9.2[d]
$GdCo_5(2c)$	-17.3	+4.1	+7.3		-5.9		+6.2[d]
$GdCo_5(3g)$	-17.8	+1.2	+9.3		-7.3		-7.2[d]

[a]Reference 14.
[b]Reference 13.
[c]Reference 12.
[d]Reference 15.

moment on the $3g$ site. Both in our FLAPW and LMTO calculation we found the opposite ordering. When they included spin-orbit coupling, Nordström *et al.* found orbital moments on the $2c$ and $3g$ sites of 0.14 and $0.10\mu_B$, respectively[52] and of 0.26 and $0.17\mu_B$ when orbital polarization was included.[53] In both cases, the orbital moment on the $2c$ site is found to be larger than the moment on the $3g$ site whereas we find them to be equal.

B. Hyperfine fields

Hyperfine field measurements have played an important role in investigations of the magnetic properties of YCo_5. The hyperfine fields at the Co sites are strongly reduced with respect to those in hcp Co, and this has been interpreted as being partly due to large orbital moments.[12,15] The anisotropy in the hyperfine fields has been related to an anisotropy in the orbital moments[13] and local anisotropy energies were then derived from these anisotropies.[13] Since our calculations are at variance with the assignment of orbital moments to the $2c$ and $3g$ sites, it is important to see whether the simple interpretation of the NMR measurements by Streever[13] is well founded.

In Table IV we list calculated hyperfine fields in YCo_5, $GdCo_5$ and Fe, Co, and Ni. The calculations for the transition-metal elements agree with previously published results that do not take OP into account.[27] The difference between the theoretical and experimental results is about 8 T for Fe, 0 T for Co, and 3 T for Ni. Including orbital polarization only increases the discrepancy due to the enlarged orbital hyperfine field. The calculated hyperfine field of hcp Co then differs from the experimental value by about 4 T.

The calculated orbital hyperfine fields in YCo_5 are twice as large as those in hcp Co. Just as the orbital moments on the $2c$ and $3g$ sites scarcely differ, there is no essential difference between the orbital hyperfine fields on these two sites. The large difference in the total hyperfine fields of -4.2 T at the $3g$ site and $+4.6$ at the $2c$ site is caused by a positive contact valence contribution to the hyperfine field at the $2c$ site rather than by different orbital moments, as has been assumed.[15] This result does not depend on whether or not the orbital polarization term is used. The total hyperfine field results from a cancellation of contact and orbital contributions and its interpretation is complicated by the polarization of the core electrons by the valence electron magnetization. There is a large spread in the values measured experimentally but irrespective of which values are chosen for comparison, it can be seen that the orbital polarization term does not lead to an improvement in the calculated values.

The hyperfine field at the $3g$ sites is quite sensitive to the RE atom. When Y is replaced with Gd (see Table IV), the valence contact term at the $3g$ site changes significantly, much more than that at the $2c$ site, resulting in nearly identical hyperfine fields at both sites in $GdCo_5$. A large discrepancy between experimental and theoretical results exists whose origin is not clear. It has been shown that orbital effects from the core electrons are negligible.[37]

C. Anisotropy energy of YCo_5

Many experiments have been carried out to attempt to explain the origin of the large magnetocrystalline anisotropy of YCo_5. We have outlined above how large orbital moments were found on the Co atoms in YCo_5, with the largest orbital moment being found on the $2c$ site, how a correlation was established between the $2c$ site and the anisotropy energy,[6] how a large anisotropy in the magnetization was attributed to the $2c$ site,[7] and how hyperfine field measurements were used to associate a local anisotropy energy with the anisotropy in the orbital moments on the $2c$ site in particular.[13] However, these conclusions about the origin of the anisotropy energy are based on some unproven assumptions such as the existence of a local anisotropy energy. In this section we describe calculations of the anisotropy energy and orbital moments within the itinerant electron model which allow us to establish a correlation between the anisotropy energy and the anisotropy in the orbital moment and study in some detail the origin of the anisotropy.

YCo_5 has $n=48$ valence electrons per unit cell. In Fig. 1 the anisotropy energy $\Delta E^n(n)$ is plotted as a function of the volume element used to perform the Brillouin-zone integral; it is seen to be well converged irrespective of whether orbital polarization is or is not included (open and filled circles, respectively). In both cases it is positive, thus favoring an orientation of the magnetization along the c axis.

In Fig. 2, $\Delta E^n(q)$ is shown for the range of band fillings $44<q<52$ (corresponding to the energy range $-2.5<\varepsilon_F(q)<-1.7$ eV). The solid and dashed curves were

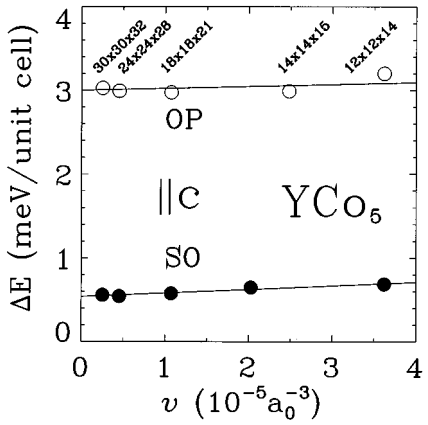

FIG. 1. Convergence of the anisotropy energy of YCo_5 as a function of the volume element v used to perform the BZ integral. The number of divisions of the reciprocal-lattice vectors corresponding to each volume are indicated at the top of the figure. The filled circles refer to calculations where only spin-orbit coupling was used (SO). The data points shown as open circles were calculated including spin-orbit coupling and orbital polarization (OP). The horizontal lines were obtained by a least-squares fit through the data points using a weight $1/v$ for each data point. Positive values of the anisotropy energy correspond to a preference for the magnetization to be oriented parallel to the c axis.

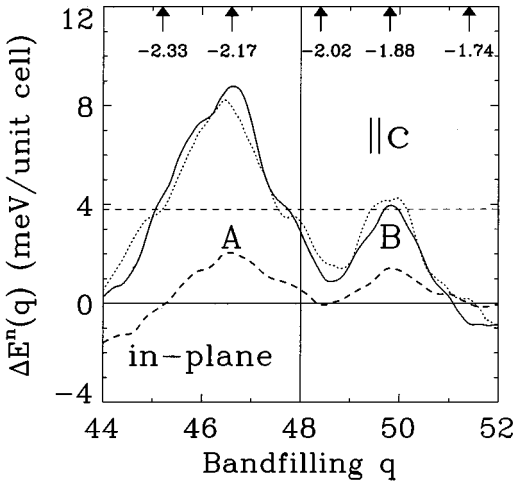

FIG. 2. Anisotropy energy $\Delta E^n(q)$ versus band filling q. Dashed curve: spin-orbit coupling only. Solid curve: spin-orbit coupling and orbital polarization (mesh $30\times30\times32$ k points). Dotted curve: spin-orbit coupling and orbital polarization (mesh $6\times6\times6$ k points). The experimental anisotropy energy is denoted by a horizontal dashed line. In the top of the figure an energy scale is denoted (in eV). The Fermi energy corresponding to $q=n=48$ is at -2.06.

both calculated using a mesh of $30\times30\times32$ **k** points in the full Brillouin zone, the densest mesh shown in Fig. 1. This corresponds to using 4097 and 1547 irreducible **k** points when the magnetization is oriented in the x and z directions, respectively. The dashed curve was obtained by including spin-orbit coupling only in the Hamiltonian, whereas to obtain the solid curve spin-orbit coupling and orbital polarization were included. Both curves exhibit two distinct peaks which are labeled A and B in the figure. We will explain the origin of these two peaks beginning with the case where only spin-orbit coupling is included.

1. Spin-orbit coupling only

For band fillings $45<q<51$ an easy axis parallel to the c axis is favored. The amplitudes of the peaks A and B are about a factor of 2 smaller than the experimentally determined anisotropy energy shown as a dashed horizontal line in the figure.[54] The magnetocrystalline anisotropy energy at a band filling corresponding to stoichiometric YCo_5, $\Delta E^n(n)$, is about a factor of 7 smaller than the experimental value. The anisotropy energy is zero when all the d bands are filled (for $q>54$). When the Fermi energy is lowered into the d band complex, we find an anisotropy energy density $\Delta\mathscr{E}^n(\mathbf{k},q)$ which varies in magnitude and sign throughout the BZ. The sign of $\Delta E^n(q)$ in general results from summing compensating contributions. In the sense that it depends on the outcome of a complicated cancellation, the sign of $\Delta E^n(n)$ is accidental. When there are degenerate bands present at a Fermi energy $\varepsilon_F(q)$, the local contributions appear and vanish when the Fermi energy is displaced by an amount comparable to the spin-orbit coupling constant. If this band degeneracy occurs over a substantial volume of the Brillouin zone then an important contribution to the anisotropy energy can result. For example, if the spin-orbit interaction $\xi_d\boldsymbol{l}\cdot\mathbf{s}$ were to split degenerate energy bands by $\pm\xi_d$, as happens for eigenstates with $m=\pm2$ character, and if 0.03 electrons participated in the splitting, this would yield a peaked structure in $\Delta E^n(q)$ with a maximum value of the anisotropy energy of 2 meV for a typical value of $\xi_d=72$ meV.

We begin with feature A in $\Delta E^n(q)$ at a band filling of $q=46.6$ [corresponding to an energy about 0.1 eV below the actual Fermi energy $\varepsilon_F(q=n)$], and then examine the changes that occur when the bands are filled with more electrons until 48 valence states are occupied. The peaked structure of this feature on the scale of ξ_d indicates that degenerate energy bands may play a role in the anisotropy energy. In order to study the anisotropy energy density $\Delta\mathscr{E}^n(\mathbf{k},q)$, the BZ was first divided into 10 slabs of thickness $0.2(\pi/c)$, parallel to the ΓKM basal plane. By integrating the anisotropy energy density in each of these slabs it was found that only a part of the Brillouin zone was responsible for most of the total anisotropy energy of 2 meV. About half of this anisotropy energy originates in the two slabs adjacent to the basal (ΓKM) plane of the BZ. The two neighboring slabs [between $\pm0.2(\pi/c)$ and $\pm0.4(\pi/c)$] together account for a quarter of the anisotropy energy. Thus 75% of the anisotropy energy is generated in 40% of the BZ. In Fig. 3 the anisotropy energy density in the two slabs adjacent to the basal plane is shown in a fishnet-contour plot representation in the $(\mathbf{G_1},\mathbf{G_2})$ plane. For each value of (k_x,k_y) the anisotropy energy density has been averaged by integrating $\Delta\mathscr{E}^n(\mathbf{k},q)$ from $k_z=-0.2(\pi/c)$ to $k_z=+0.2(\pi/c)$ and smoothing with a Gaussian to allow the result to be plotted. The positive sign of the anisotropy energy is seen to be determined by the band structure at and in the vicinity of the high-symmetry point K and along and around the high-symmetry lines ΓK and ΓM.

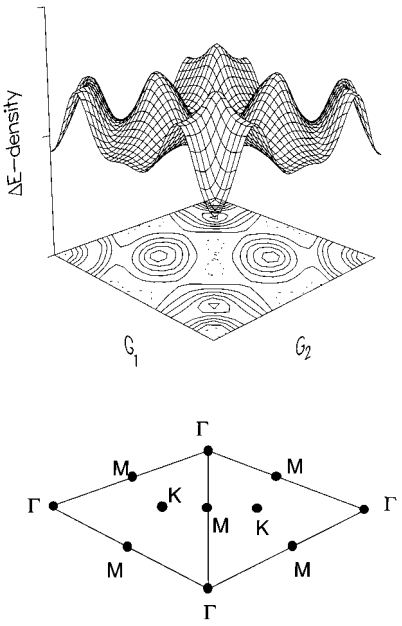

FIG. 3. Anisotropy energy density (from a calculation with spin-orbit coupling) in the basal plane of the Brillouin zone obtained by averaging over a slab of thickness $0.4(\pi/c)$, for a Fermi energy of -2.17 eV which corresponds to a band filling of $q=46.6$ and the peak A in Fig. 2. Solid (dashed) contours represent positive (negative) contributions to the anisotropy energy, respectively. Mainly K, ΓK, and ΓM contribute to the preference for a magnetization direction along the c axis.

In Fig. 4 the band structure of the majority-spin (left panel) and the minority-spin (right panel) electrons is shown along the high-symmetry lines in the basal plane. The Fermi energy is denoted by the horizontal dashed line at -2.06 eV. Within 0.5 eV of the Fermi energy a set of Co minority-spin d bands is separated from the remaining Co d bands.

The d orbital character of the minority-spin bands in the energy interval $-2.5<\varepsilon<-1.7$ is shown in Fig. 5 in a representation where the thickness of an energy band is proportional to the orbital character. Because the free-electron-like spf character in this energy range is small and fairly uniform, it is not shown. There are six columns, one for each atom in the unit cell and five rows, which are labeled according to the d orbital character: $d_{3z^2-r^2}$, $d_{x^2-y^2}$, d_{yz}, d_{xz}, and d_{xy}. For an arbitrary $\mathbf{k}$ point there is no relationship between the orbital character on crystallographically equivalent atoms. The symmetry of the ΓKM direction shown is such that the two Co($2c$) atoms are equivalent and the first and second Co($3g$) atoms are also equivalent. We anticipate our main conclusions by noting that the states which make the most important contribution to the MAE of YCo_5 are the states with mainly $d_{x^2-y^2}$ and d_{xy} character which are doubly degenerate at the K point at -2.2 eV and at the Γ point where they are almost degenerate with the Fermi energy. The states at K have mainly Co($3g$) but also some Co($2c$) character, those at Γ have mixed Co($3g$) and Co($2c$) character.

When the spin-orbit coupling is included, the energy bands in this energy range display pronounced differences if the magnetization is directed along or perpendicular to the c axis. In Fig. 6 the minority-spin band structure (in the absence of spin-orbit coupling) and the band structures from which the anisotropy energy density was generated are shown along lines of high symmetry for two directions of the magnetization. Correlating plots of the anisotropy energy density as shown in Fig. 3 with these band structures shows that if the magnetization is directed along the c axis, there is a net energy gain from the splitting of the encircled energy bands because the bands which are shifted to higher energies by the spin-orbit interaction are unoccupied. Thus the encircled energy bands at the K point are the states mainly responsible for the preference for a c-axis-oriented magnetization for this band filling.

In the absence of spin-orbit coupling, these bands are doubly degenerate at an energy $\varepsilon=-2.20$ eV and have mainly Co-d $m=\pm 2$ character (i.e., $d_{x^2-y^2}$ and d_{xy} symmetry). These states are split by the spin-orbit coupling to $\varepsilon=-2.27$ eV and $\varepsilon=-2.13$ eV if $\mathbf{n}\|c$, and are left nearly degenerate if $\mathbf{n}\perp c$. We expect the contribution to the anisotropy energy from these two states in the vicinity of K to be maximal at $\varepsilon=-2.20$ eV, and to vanish at $\varepsilon=-2.33$ eV and -2.11 eV. This positive contribution to the anisotropy energy density can be seen in Fig. 3. There is a similar contribution to the anisotropy energy from two bands which were nearly degenerate in the absence of spin-orbit coupling from Γ to nearly halfway along ΓK and ΓM.

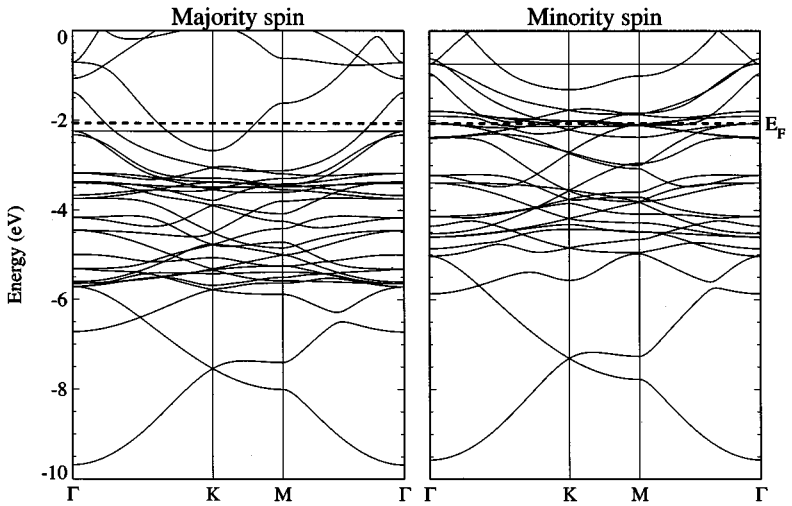

FIG. 4. Energy bands without spin-orbit coupling along the high-symmetry lines in the basal plane of the BZ, for the majority-spin electrons (left panel) and the minority-spin electrons (right panel). The Fermi energy is indicated by the dashed horizontal line.

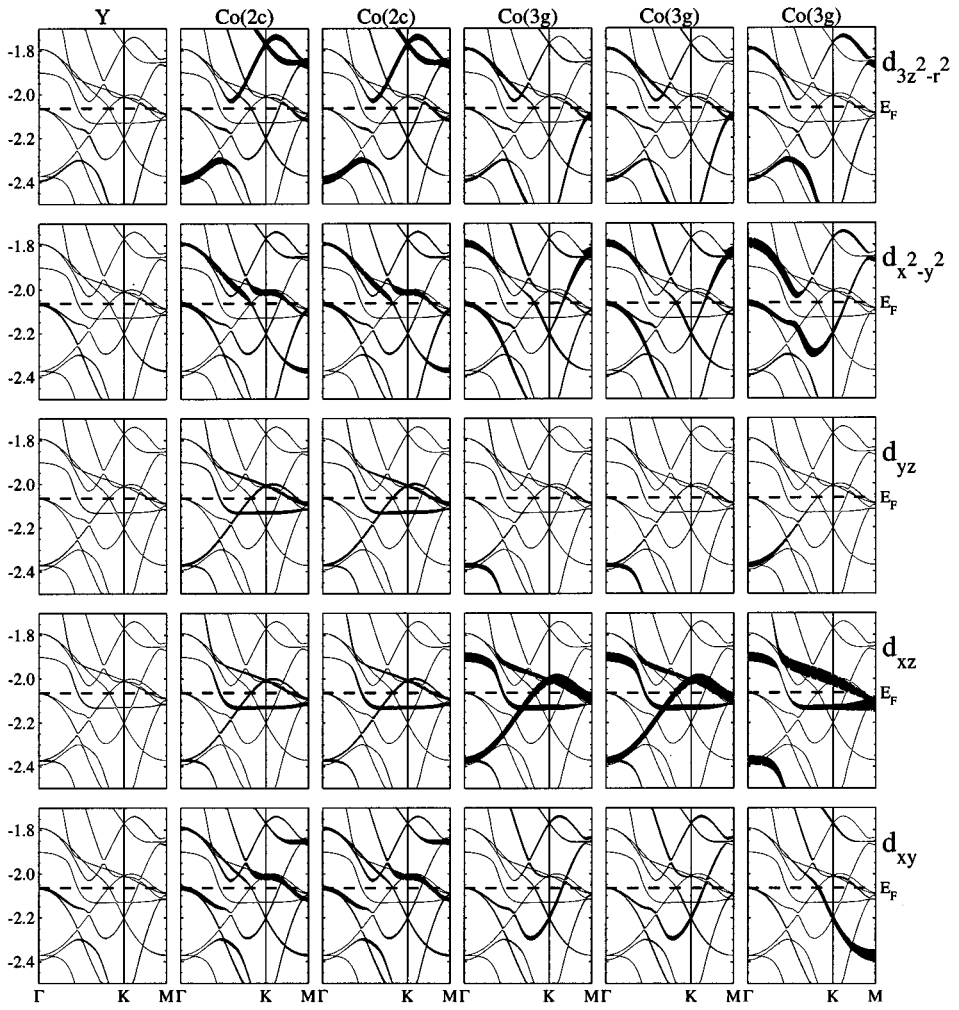

FIG. 5. The orbital character of the minority-spin energy bands along the lines ΓK and KM in the energy interval $-2.5<\varepsilon<-1.7$ is indicated for the six atoms in the unit cell (columns). The thickness of the band is proportional to the orbital character (there is a minimum thickness, however). The Fermi energy is indicated by the dashed horizontal line.

At Γ, these two states are degenerate in the absence of spin-orbit coupling; they are also indicated by filled circles in Fig. 6. They lie very close to the Fermi energy $\varepsilon_F(q=48)$ and their splitting provides the only large contribution to the anisotropy energy from in or around the ΓKM plane which favors a c-axis orientation of the magnetization (see Fig. 7). The contributions from K, ΓK, and ΓM are seen to favor an in-plane magnetization for this band filling. The positive anisotropy energy from around Γ is compensated by a negative anisotropy energy from the remainder of this slab with the anisotropy energy of the total slab being negative. The reason why the anisotropy energy is still positive at $q=48$ (Fig.

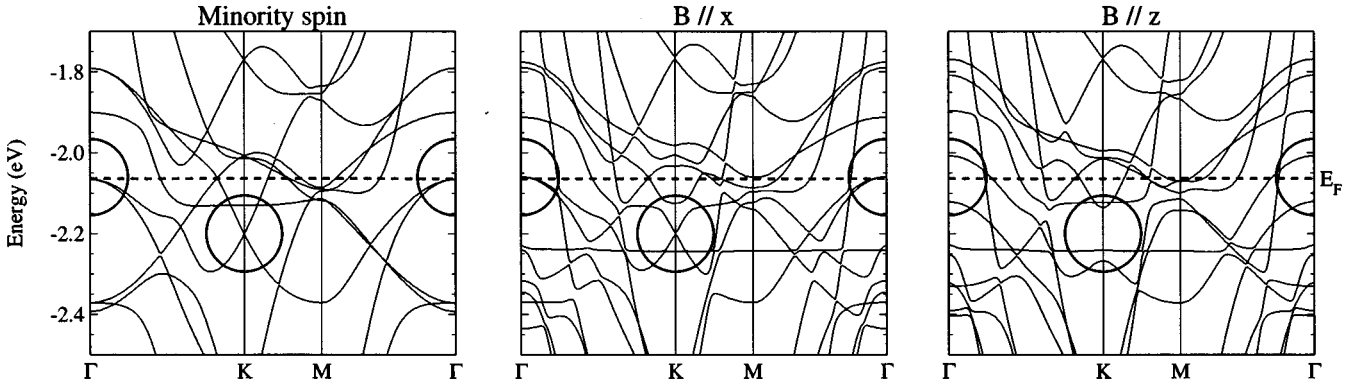

FIG. 6. Influence of the magnetization direction on the energy band splittings when spin-orbit coupling is included. The minority-spin energy bands are shown in the left-hand panel for reference. Right-hand panel: magnetization direction along the c axis. Middle panel: magnetization in the ΓM direction. The splittings of the states which are encircled are discussed in the text. The Fermi energy is indicated by the dashed horizontal line.

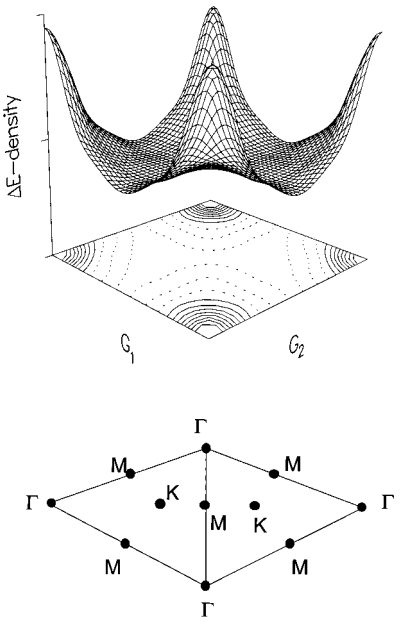

FIG. 7. See the figure caption of Fig. 3. The anisotropy energy density is plotted for the actual Fermi energy of -2.06 eV, corresponding to a band filling of $q=48$. Only Γ and a small region around it make a positive contribution to the MAE (favoring a c-axis orientation).

2) is that there is a positive contribution from the neighborhood of the (AHL) planes of the BZ. Finally, raising the Fermi energy even further to 0.18 eV, corresponding to a band filling of $q=49.8$ (peak B in Fig. 2), the positive anisotropy energy is generated in the 40% of the zone adjacent to the AHL plane. It is related to the lifting of a double degeneracy at the H point.

2. Spin-orbit coupling and orbital polarization

The influence of spin-orbit coupling and orbital polarization is maximal in the special situations when degenerate energy bands with $m=\pm 2$ character occur, as at Γ and K, and when $\mathbf{n}$ is parallel to c. Because the dependence of the minority-spin minority-spin block of the Hamiltonian on the direction of the magnetization is $(BL+\frac{1}{2}\xi_d)\boldsymbol{l}\cdot\mathbf{n}$, the orbital polarization term in the Hamiltonian essentially represents an enhancement of the spin-orbit coupling parameter. With a Racah B parameter of about 0.14 eV, and $L=0.23$, the orbital splitting factor BL is about equal to the spin-orbit splitting $\frac{1}{2}\xi_d=0.036$ eV. When orbital polarization is included in the calculations, the overall shape of $\Delta E^n(q)$ is unchanged (Fig. 2). However, the amplitude of the anisotropy energy curve increases by about a factor of 4, consistent with a ξ^2 estimate for the dependence of the anisotropy energy on ξ, using perturbation theory for uniaxial systems.[55] The calculated anisotropy energy of YCo_5 of about 3 meV/unit cell is in quite good agreement with the experimental value of 3.8 meV/unit cell.

The spin-orbit coupling gives rise to an anisotropy in the magnetic moment which is also enhanced by the orbital polarization. In Fig. 8 the anisotropy in the magnetic moment and its decomposition into an orbital moment anisotropy and a spin moment anisotropy is shown as a function of the band filling. Typically, the anisotropy in the orbital moment is

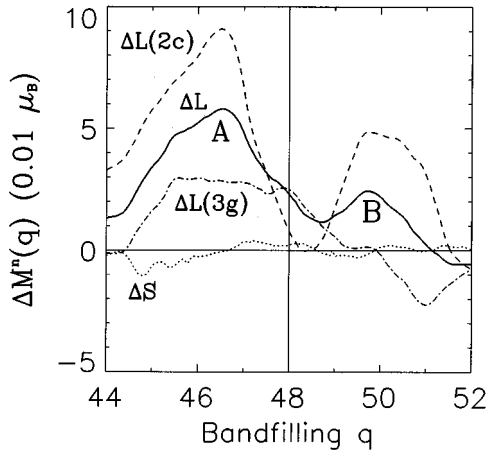

FIG. 8. Anisotropy in the magnetic moment as a function of the band filling q. The anisotropy in the orbital moment per Co atom is shown as a solid line, the anisotropy in the spin moment per Co atom as a dotted line. The dashed and chain-dashed curves are the anisotropy in the orbital moment of a Co $(2c)$ atom and a Co $(3g)$ atom, respectively.

about a factor of 5 larger than the anisotropy in the spin moment. Projecting out the anisotropy in the orbital moment onto the Co atoms at the $2c$ and $3g$ sites as a function of the band filling, peaks A and B are seen to be mainly attributable to the Co atoms at the $2c$ sites. For example, at peak A the anisotropy in the orbital moment of a Co atom at the $2c$ and $3g$ site is 0.09 and $0.03\mu_B$, respectively. The difference in the anisotropy for the two types of Co atoms is even more pronounced at peak B, where the anisotropy is almost entirely due to that of the Co atoms at the $2c$ sites. However, at the Fermi energy of YCo_5 $(q=48)$, the situation is reversed and the anisotropy in the $2c$ site orbital moment is negligible. For $q=48$ the anisotropy in the total magnetic moment is calculated to be $0.13\mu_B$ per unit cell. This anisotropy has been measured[7] and found to have a value of $0.31\mu_B$ per unit cell.

The similarity between the $\Delta E^n(q)$ and the $\Delta L^n(q)$ curves is striking, and allows us to decompose the anisotropy energy into site-dependent contributions. Using perturbation theory for uniaxial systems, a roughly linear relation between the anisotropy energy and the anisotropy in the orbital moment is expected,[56,26] with a proportionality factor of $\frac{1}{4}\xi_d$, or, in the case of orbital polarization, $\frac{1}{2}(BL+\frac{1}{2}\xi_d)\sim\frac{1}{30}$ eV. In the case of degenerate energy bands, one expects a proportionality factor which is about a factor of 2 larger. Although the ratio $\Delta E^n(q)/\Delta L^n(q)$ certainly is not constant, it is generally of this order of magnitude.

The large measured orbital moments have been thought to be associated with a strong asphericity in the spin density of the Co atoms at the $2c$ sites.[10] Experimentally, about 60% of the spin density was found to have $m=\pm 2$ character. In Sec. III A we already discussed that this is not found in the calculations. However, there is a large density of $|m|=2$ states just below the Fermi energy. In Fig. 9 the minority Co d density of states is shown as a function of the band filling. The Fermi energy corresponding to $q=48$ states is located on the edge of a steep peak in the density of states (DOS), which extends from about 45.8 to 48.5 filled valence states. The peak consists of 54% Co $(2c)$ character and 46% Co

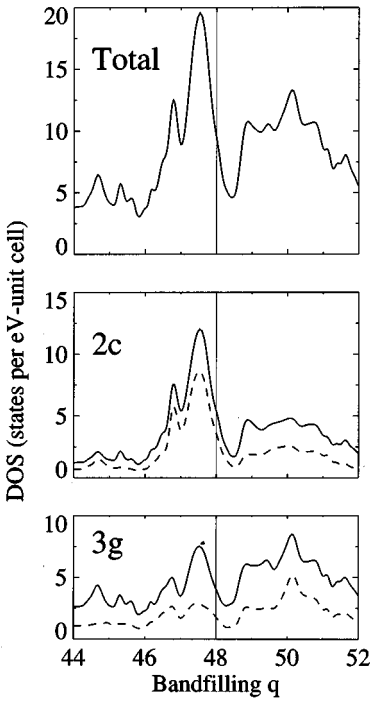

FIG. 9. Cobalt minority-spin d partial density of states (DOS) for a calculation without spin-orbit coupling or orbital polarization, as a function of the band filling q. The solid curves are the total Co d DOS, the total Co $(2c)$ d DOS and the total Co $(3g)$ d DOS. Dashed curves are the Co $(2c)$ and $(3g)$ $m=\pm 2$ projected DOS. The two peaks in the total DOS below the Fermi level (denoted by the vertical lines) have mainly Co $(2c)$ $m=\pm 2$ character.

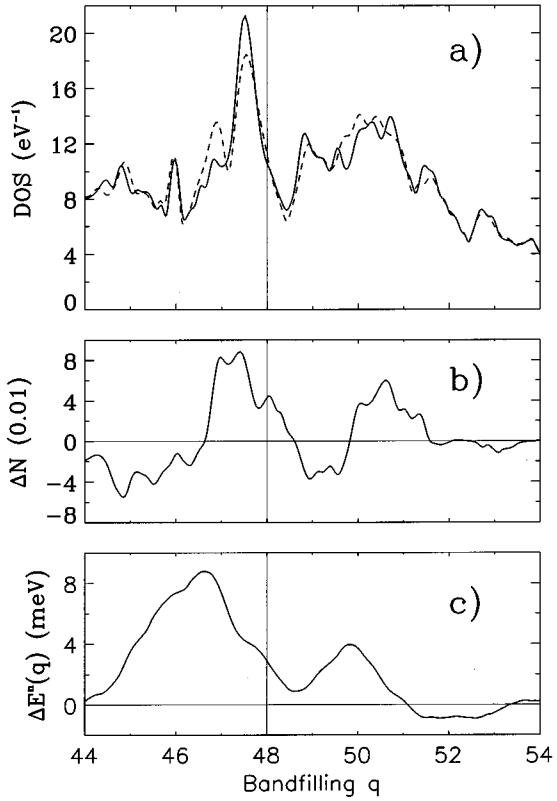

FIG. 10. (a) Total density of states for calculations including spin-orbit coupling and orbital polarization with the magnetization direction along the c axis (solid curve) and in plane (dashed curve) in units of states per eV per unit cell, versus the band filling q of each calculation. (b) Integral of the density of states calculated with the magnetization in-plane up to the Fermi energy $\varepsilon_F(q)$ of the c-axis calculation, minus q, the number of occupied valence states of the c-axis calculation, as a function of q. (c) The anisotropy energy as a function of q.

$(3g)$ character, rather than the expected values of 40 and 60 %, respectively which one would expect from a simple concentration dependence. The partial DOS shows that about 65% of the Co $(2c)$ d DOS has $m=\pm 2$ character, much more than the 40% which would occur if all five d orbitals were equally populated. The Co $(3g)$ d DOS has about 45% $m=\pm 2$ character. That there is a strong peak in the d DOS between $q=45.8$ and 48.5 valence states with predominant Co $(2c)$ $m=\pm 2$ character does not by itself explain the preference for the c-axis orientation. In Fig. 10(a) the density of states as a function of the band filling is shown for calculations including spin-orbit coupling and orbital polarization, where the magnetization direction is directed along the c axis (solid curve) and perpendicular to the c axis (dashed). The most obvious difference is the vanishing of the peak in the DOS at $q=46.8$, when the magnetization is rotated from in-plane to being parallel to the c axis. The ''missing'' states are distributed to lower and higher energies. Most of this partial density of states has $m=\pm 2$ character. If each density of states is integrated to a common energy, $\varepsilon_F(q)$ of the c-axis calculation, the redistribution of the density of states by the spin-orbit interaction and the orbital polarization leads to a different number of occupied valence states at that energy for the two field directions. The difference in the number of occupied states at the energy $\varepsilon_F(q)$ between the in-plane calculation and the c-axis calculation is plotted as a function of the c-axis band filling q in Fig. 10(b). The larger and smaller number of states, below and above $q=46.6$, respectively, for the c-axis calculation versus the in-plane calculation is the cause of the increase and decrease of the anisotropy energy versus band filling, shown in Fig. 10(c). The difference in the number of states varies on an energy scale of the order of $2(BL+\frac{1}{2}\xi_d)$.

Finally, we note that the dipole-dipole anisotropy energy yields a small preference for the c-axis magnetization of 0.05 meV/unit cell, about 1% of the magnetocrystalline anisotropy energy. It may therefore be neglected.

3. Symmetry point analysis of the anisotropy energy

It appears from the discussion in the previous two sections that points of high symmetry play a particularly important role in determining the anisotropy energy. In earlier work[33] we found that it was possible to explain the most important features in $\Delta E^n(q)$ in terms of the effect of the spin-orbit coupling on the states at the points of high-symmetry only. If we compare $\Delta E^n(q)$ calculated with a mesh of $6\times 6\times 6$ **k** points (corresponding to a total of 80 irreducible **k** points) with the results for the $30\times 30\times 32$ mesh calculation, then we see in Fig. 2 that all of the important features are reproduced very well using the smallest regularly spaced mesh which includes all of the points of high symmetry. We will now show that the most important

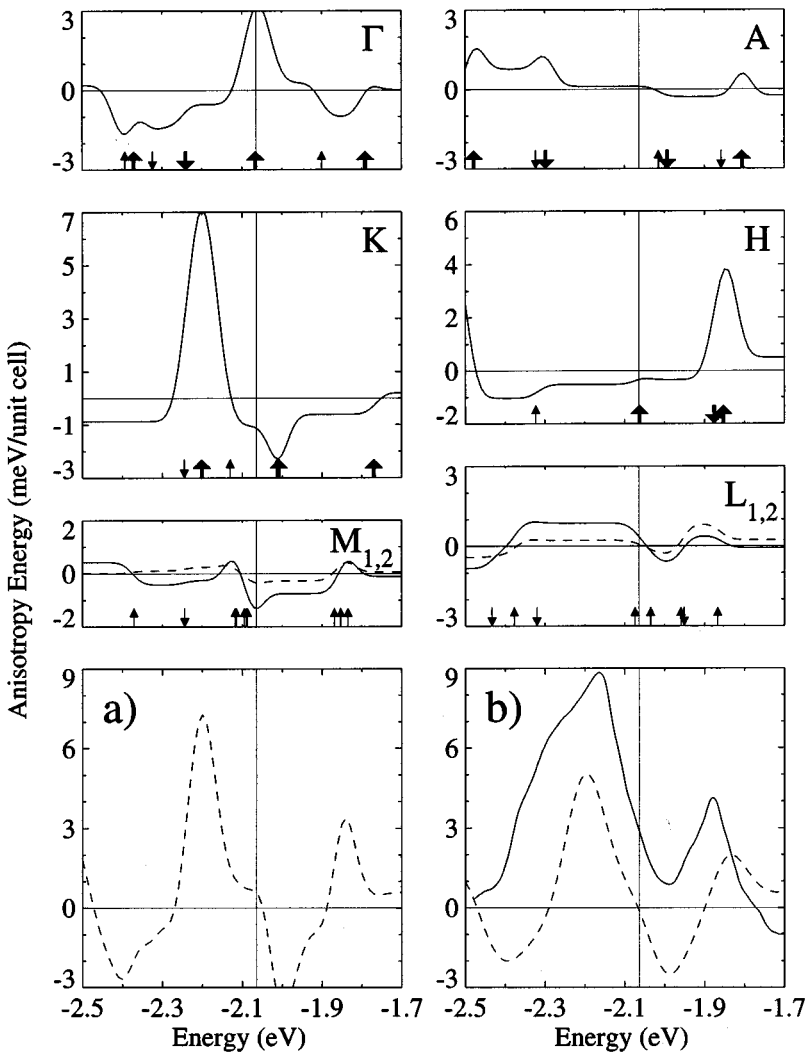

FIG. 11. Anisotropy energy of YCo_5 contributed by the high-symmetry points Γ, K, M, A, H, and L as a function of energy corresponding to variable band filling of the fixed band structure. The weight factor, $w_{\mathbf{k}}$, is included. The upward (downward) pointing arrows indicate the position of the minority- (majority-) spin energy levels in the absence of spin-orbit coupling. Thin and thick arrows are used to denote singly and doubly degenerate eigenstates, respectively. For the M and L points, the subscripts 1 and 2 refer to the solid and dashed curves, respectively. The dashed curve in the bottom panel (a) is the result of adding the contributions of these **k** points. The dashed curve in panel (b) is obtained by an additional broadening using a Gaussian with a width of 0.1 eV. The solid curve results from a calculation where a total of 5644 ($=4097+1547$) irreducible **k** points was used. The actual Fermi energy is denoted by the vertical line at -2.06 eV.

qualitative features of the anisotropy energy curve can be understood in terms of an even smaller number of **k** points, namely, the high-symmetry points Γ, K, M, A, H, and L *only*. The contributions to the anisotropy energy from these **k** points are shown in the top six panels of Fig. 11. The arrows in Fig. 11 indicate the positions of the energy levels at each **k** point, and a thick arrow denotes degenerate energy levels (in the absence of spin-orbit interaction). Upward (downward) pointing arrows denote minority (majority) spin eigenstates. The anisotropy energy at each **k** point is broadened using a Gaussian with a width of 0.06 eV, and multiplied with a weight factor $w_{\mathbf{k}}$. The total anisotropy energy curve, shown in the bottom left panel, is obtained by summing the weighted contributions from each **k** point. The weight factor of a particular **k** point is determined by its number density in the BZ. If the magnetization direction is chosen parallel to the x axis (parallel to the reciprocal-lattice vector $\mathbf{G}_2$), then the two K points in the BZ, $\frac{1}{3}(\mathbf{G}_1+\mathbf{G}_2)$ and $\frac{2}{3}(\mathbf{G}_1+\mathbf{G}_2)$, are equivalent. One of the M points, $M_2=\frac{1}{2}\mathbf{G}_2$, is not equivalent to the other two M points, $\frac{1}{2}\mathbf{G}_1$ and $\frac{1}{2}(\mathbf{G}_1+\mathbf{G}_2)$, denoted by M_1. The same is true of the H and L points, respectively. The contributions from the inequivalent M_1 and L_1 (M_2 and L_2) points are indicated by the solid (dashed) curves. The weight factors for the special points Γ, K, M_1, and M_2, (and similarily for A, H, L_1, and L_2) are then chosen as 1/12, 1/6, 1/6, and 1/12.

Broadening the curve in Fig. 11(a) with a Gaussian of width 0.1 eV yields the dashed curve in Fig. 11(b), which has a similar functional dependence on the band filling as the full calculation, represented by the solid curve, but differs by a roughly constant amount. The origin of the two peaks, A and B, in the lifting of degeneracies at K and H, respectively, is made particularly clear in this analysis. The origin of the discrepancy between the two curves in Fig. 11(b) can be found by examining Fig. 3. We see that there is a large positive contribution to the MAE from an annular region about Γ but that the contribution from the Γ point itself is negative. The dotted curve in Fig. 2 shows that an only slightly better sampling is required to correct for this error.

In this work and in earlier work[33] we have found that the lifting of degeneracies at points of high-symmetry and along symmetry lines makes an important contribution to the magnetocrystalline anisotropy energy. In uniaxial systems two situations may arise which are illustrated in Fig. 12. There we sketch the energy band dispersion $\varepsilon_{\mathbf{k}_{//}}$ as a function of the in-plane k vector $\mathbf{k}_{//}$ of two states in the vicinity of a point of high symmetry where the two states are degenerate in the absence of spin-orbit coupling. The states with $m=\pm 2$

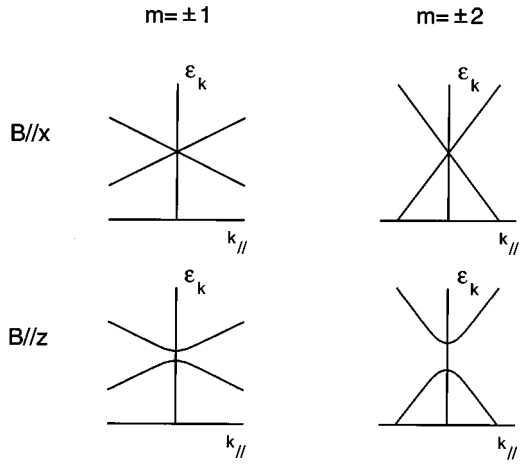

FIG. 12. An illustration of two situations which may arise in systems with uniaxial symmetry. The energy band dispersion in the vicinity of a point of high symmetry where a degeneracy occurs is sketched for the case where the two states have $m=\pm 1$ character and a small dispersion (left-hand side) and the case where the two states have $m=\pm 2$ character and a large dispersion (right-hand side). When spin-orbit coupling is included and $B//x$, the degeneracy is not lifted. When $B//z$ the degenerate states are split by $\pm m\xi_d/2$.

character ($d_{x^2-y^2}$ and d_{xy}) have more dispersion than the states with $m=\pm 1$ character (d_{yz} and d_{xz}) as a consequence of their spatial form and the resulting greater or lesser overlap between orbitals on neighboring atoms. When spin-orbit coupling is included the degeneracy is lifted when the magnetization is oriented along the z axis. The splitting, which is $\pm m(\xi_d/2)$, is largest for the states with the greatest dispersion. It is not obvious which situation will have the largest anisotropy energy: a smaller splitting over a larger volume of reciprocal space (as a result of the smaller dispersion) or a larger splitting over a smaller volume of reciprocal space. In this work and our earlier work we have found that states with $m=\pm 2$ character play a more important role.

Peak A in $\Delta E^n(q)$ (Fig. 2) tells us something very important, namely, that magnetic anisotropy energies substantially larger (in this particular case, two times larger) than those found for YCo_5 can, in principle, be found in itinerant magnets, i.e., without having to make recourse to compounds which contain rare-earth ions. Before embarking on the search for materials with larger coercivities, it is very important to know that there is no principle which states that even harder magnetic materials, harder than the best obtainable nowadays, are not possible.

4. Comparison with previous work

Nordstrom *et al.*[53] have calculated the MAE of YCo_5 making essentially the same approximations as we have made and reaching essentially the same qualitative conclusions. However, some of the technical details of their LMTO-ASA calculations were different, as we saw earlier when discussing the magnetization, and this results in some significant quantitative differences. For example, these authors did not obtain well converged values of the MAE integral. Including spin-orbit coupling only, they found values of the MAE which were positive (thus favoring a c-axis orientation) for three different finite integration meshes. The value obtained by extrapolating to infinitesimal volume was, however, negative. The best value of the MAE obtained with spin-orbit coupling and orbital polarization was a factor of 2 smaller than the experimental value and there was a very large uncertainty in this value. By using the improved tetrahedron method,[31] we have a very small (numerical) uncertainty in our values of the MAE as can be seen in Fig. 1.

D. Electric-field gradient, crystal-field parameters, and exchange field

The electric-field gradient (EFG) and the crystal-field parameter A_2^0 at the RE site are determined by the electrostatic potential at or close to the nucleus; the EFG is determined by the anisotropy in the electrostatic potential at the nucleus while the $4f$ crystal field splitting is determined by the sampling of the electrostatic potential around the maximum in the $4f$ radial wave functions which is about 0.5 a.u. from the nucleus. If the charges which give rise to the potential do not overlap the $4f$ charge density as, for example, in a point charge model, then the second-order crystal-field parameter is proportional to the electric-field gradient with a proportionality factor $-\frac{1}{4}e$. For example, $V_{zz}=10^{20}$ V/m^2 would correspond to $A_2^0=-812K/a_B^2$. In this section the EFG and crystal-field parameters calculated for $GdCo_5$ are compared with experimental results and the contributions to both quantities analyzed. We also report the value of the exchange-field coupling rare-earth and valence electron spins as calculated within the LSDA.

1. V_{zz}

Blaha *et al.*[44] have calculated the EFG's for a number of hcp elements using the method outlined in Sec. II D. Without using any free parameters, they obtained agreement with experimental values to within typically 20% which is of the order of the experimental uncertainty. The lattice contribution was found to be only about 10–20 % of the on-site (valence) value and had the opposite sign. Making a number of additional approximations, Coehoorn *et al.*[57] calculated the on-site contribution to the EFG and obtained similar results for the hcp metals as Blaha *et al.* thus confirming indirectly the smallness of the lattice contribution. We have tested our computer code by calculating the EFG's for a number of the hcp metals treated in Ref. 44 and find agreement with the results reported there.

Fewer calculations have been performed for compounds. Blaha *et al.*[58] calculated the EFG's for the three inequivalent sites in the ionic compound Li_3N and found agreement with experiment to within better than 20%. The lattice contribution was found to make an important contribution to V_{zz} but the EFG's themselves were quite small, $\sim 10^{21}$ V/m^2. Using the same approximations which he used for the hcp metals, where the lattice contribution is expected to be small because all atoms are equivalent, Coehoorn calculated the EFG's on the Gd site for a number of metallic compounds GdT_2X_2 with the $ThCr_2Si_2$ structure.[57] Again there was agreement between theory and experiment to within about 20% unless T was a $3d$ element where the agreement was generally poorer. Similar results were found for a number of intermetallic compounds[59] where for $GdCo_5$ in particular, a value of

TABLE V. Electric-field gradient in $GdCo_5$ separated into the on-site and lattice contribution, in units of 10^{21} V/m^2. The on-site contribution is analyzed in a *5p-5p* semicore contribution and *6p-6p* and *5d-5d* valence electron contributions.

	On-site	Lattice	Total	Expt.
Semicore *5p-5p*	−3.3			
6p-6p	18.7			
5d-5d	2.4			
Others	0.6			
	18.4	−0.1	18.3	8.2 [a];9.7[b]

[a]Reference 17.
[b]Reference 16.

14×10^{21} V/m^2 was calculated for V_{zz} compared to experimental values of 9.7×10^{21} V/m^2 reported by Steenwijk *et al.*[16] and 8.2×10^{21} V/m^2 reported by Tomala *et al.*[17] The larger discrepancies found for these compounds raise the question as to whether the neglected lattice contribution is more important in these materials. However, we should note that the discrepancies are substantially larger than the lattice contributions found in the ionic compound Li_3N.

The results of our calculations of the EFG of Gd in $GdCo_5$ are given in Table V. The calculated EFG is about a factor of 2 larger than the measured value and the discrepancy is even bigger than that found by Coehoorn. In the table, the EFG is split up into a number of different contributions. The contribution of the semicore states was calculated by taking the self-consistent charge density (obtained using $6p$ valence states and $5p$ core states) and treating the $5p$ states as bands in one iteration. As these semicore bands are split off from the valence bands, the $5p$ charge density states can be obtained easily, yielding a contribution of -18% to the EFG. The contribution of the $5p$ states to the EFG hardly changes if, treated as bands, they are iterated to self-consistency. Thus the semicore contribution is not sensitive to the detailed shape of the potential.

The EFG may be further analyzed in terms of lattice and on-site contributions as defined in Eq. (15). The lattice contribution is only 10^{20} V/m^2, or less than 1% of the EFG, which reflects the small deviation from charge neutrality of the atoms. The physical origin of the EFG lies in the deviation from spherical symmetry of the valence charge density on the Gd site. This nonspherical charge density can be resolved into $l-l'$ contributions for each spin direction (an $l-l'$ contribution to the charge density is constructed from partial waves within the muffin-tin sphere with angular momentum l and l', respectively). 98% of the EFG comes from p-p and d-d contributions to the charge density, where the latter is about a factor of 8 smaller than the former. This result is similar to that found by Coehoorn *et al.* for the Gd compounds with the $ThCr_2Si_2$ structure.

These ''diagonal'' contributions can be broken down further into terms which describe the asymmetry of the p_x, p_y, and p_z and of the $d_{x^2-y^2}$, d_{xy}, d_{xz}, d_{yz}, and $d_{3z^2-r^2}$ occupation numbers and terms which only involve radial integrals.[44,57] However, the occupation numbers and the normalization of the radial wave functions depend on the somewhat arbitrary choice of muffin tin (or atomic-sphere[57,59]) radius. The dominance of the p-p contribution to the EFG suggests that the origin of the discrepancy with experiment should be sought here.

TABLE VI. Crystal-field parameters in $GdCo_5$ separated into on-site and lattice contributions in units of K, together with the expectation values of the radial $4f$ wave function (in Bohr atomic units). The on-site contribution has been separated into a *5p-5p* semicore contribution and valence electron contributions.

(lm)	$\langle r^l\rangle$		$A_l^m\langle r^l\rangle$			
			On-site	Lattice	Total	Expt.
(20)	0.93	Semicore *5p-5p*	87			
		6p-6p	−407			
		5d-5d	−775			
		Others	−648			
		Sum	−1743	980	−763	−180[a] −420[b] −210[c]
(40)	2.11		−3	−24	−27	
(60)	8.58		0.5	3.1	3.6	
(66)	8.58		0.3	99	99	

[a]Reference 1.
[b]Reference 2.
[c]Reference 3.

2. A_l^m

The calculated crystal-field parameters are given in Table VI, separated into on-site and lattice contributions. The on-site contribution to the dominant $A_2^0\langle r^2\rangle$ term is further broken down into contributions from the different partial waves. Because the lattice contribution to $v_{l\alpha}$ is strictly proportional to r^l, the lattice contributions to A_2^0 [Eq. (14)] and to V_{zz} are related by the proportionality factor $-(e/4)$. Whereas this contribution to V_{zz} was very small, it is very important to include it in a calculation of the crystal-field parameters. The lattice contribution to A_2^0 is half as large as the on-site contribution but has the opposite sign. There is a modest $5p$ semicore contribution to A_2^0 which accounts for about 10% of the total value. The contribution of the $6p$ electrons to A_2^0, though sizeable (25% of the on-site value), is much less dominant than in the case of V_{zz}. The $5d$-$5d$ charge density accounts for about 45% of the on-site value for A_2^0. $5f$-$5f$, $6p$-$5f$ and $5d$-$5g$ terms mainly make up the contribution labeled ''others.'' The calculated value of A_2^0 is a factor 2–3 larger than the values derived from crystal-field calculations of the single-ion anisotropy energy which give the best agreement with experiment.[1–3] A_2^0 changes by only about 10% if the $4f$ states are treated as itinerant electrons (which is possible for the special case of Gd). Moreover, we expect our results for A_2^0 obtained for $GdCo_5$ to be valid for most of the RE atoms. The discrepancy with experiment may be due to non-Hartree contributions to the single-particle potential, or to the apparent difficulty in obtaining a reliable experimental

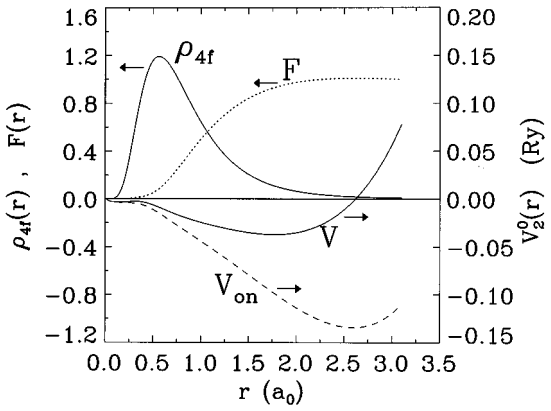

FIG. 13. Radial dependence of the $l=2$, $m=0$ component of the total Coulomb energy $V_2^0=(-e)v_{20}$ and the on-site contribution V_{on} to the Coulomb energy in Rydbergs referred to the right-hand axis. r, the distance to the nucleus is in Bohr atomic units. The normalized $4f$ charge density, $\rho_{4f}(r)=4\pi r^2\phi_{4f}^2(r)$, and the integral $F(r)=I(r)/I(R)$, where $I(r)=\int_0^r\rho_{4f}(x)V_2^0(x)dx$, are shown referred to the left-hand axis (in atomic units and dimensionless units, respectively). R is the muffin-tin radius. The difference between the on-site and Coulomb potential, which is $\sim r^l$, is the lattice potential. The integral $F(r)$ reaches 80% of its final value within a distance of 1.5 a.u. from the nucleus.

value. The influence of the nonspherical $4f$ charge density on the valence electron charge density should be studied carefully.

Where the lattice contribution to the potential is already very important for A_2^0, it becomes even more so for the higher order crystal-field coefficients; over 80% of the value for A_4^0 and A_6^0 comes from the lattice contribution. This may be seen in Figs. 13 and 14, where the on-site contribution to

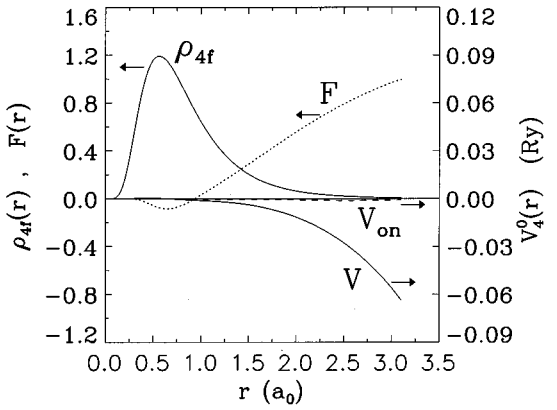

FIG. 14. Radial dependence of the $l=4$, $m=0$ component of the total Coulomb energy $V_4^0=(-e)v_{4,0}$ and the on-site contribution V_{on} to the Coulomb energy in Rydbergs referred to the right-hand axis. r, the distance to the nucleus is in Bohr atomic units. The normalized $4f$ charge density, $\rho_{4f}(r)=4\pi r^2\phi_{4f}^2(r)$, and the integral $F(r)=I(r)/I(R)$, where $I(r)=\int_0^r\rho_{4f}(x)V_4^0(x)dx$, are shown referred to the left-hand axis (in atomic units and dimensionless units, respectively). R is the muffin-tin radius. The difference between the on-site and Coulomb potential, which is $\sim r^l$, is the lattice potential. The integral $F(r)$ reaches only 30% of its final value at a distance of 1.5 a.u. from the nucleus.

the Coulomb potential energy, $V_{on}=(-e)[4\pi/(2l+1)]U_{l0}(r)$, and the total Coulomb potential energy, $V_l^0(r)=(-e)v_{l0}(r)$, are shown as a function of the distance from the nucleus, r. The difference between these two terms is the lattice contribution which scales as r^l for an A_l^m crystal-field parameter. The $4f$ radial charge density, normalized so that $\int_0^R\rho_{4f}(r)dr=1$, is shown together with the ratio $F(r)=I(r)/I(R)$, where $I(r)=\int_0^r\rho_{4f}(x)V_l^0(x)dx$. The curve $F(r)$ shows that 80% of the A_2^0 parameter is accounted for by the integral within 1.5 atomic units of the nucleus. On the other hand, only 30% of the fourth-order crystal-field parameter is generated within the same volume. The magnitude of the fourth-order crystal-field parameter is determined by the overlap of the tail of the $4f$ radial wave function with the r^l lattice potential, while the on-site contribution to the potential is negligible.

The large influence of the lattice potential on the crystal-field parameters indicates that a self-consistent calculation of the nonspherical potential is important. By performing first a self-consistent warped muffin-tin calculation (yielding a potential which is spherically symmetric within the muffin-tin sphere and which is represented by a plane-wave expansion in the interstitial region), and then taking the full nonspherical output charge density from a single iteration, we find that the EFG is given quite accurately (within 5% of the self-consistent value). However, the crystal-field parameters calculated in the same way differ from the values calculated with a fully self-consistently calculated charge density by a factor of 2. Whereas the on-site potential is described reasonably well, the lattice potential which should ensure continuity of the potential, has not yet reached its converged value.

In a recent paper, Richter *et al.*[60] have carried out a calculation of $A_l^m\langle r^l\rangle$ for $SmCo_5$ and, in order to compare with our results,[28] also for $GdCo_5$. The basic approximations which they make are the same. They work within the local-spin-density approximation and adopt a perturbative approach to describe the interaction between the atomiclike $4f$ configuration with the self-consistently calculated valence electron density. Their calculation was based upon a linear combination of atomic orbitals band structure formalism which makes it difficult to carry out a detailed comparison of the results. For $GdCo_5$ they find a value of $A_2^0\langle r^2\rangle$ of -950 K compared to our value of -763 K. The agreement for the higher l values of $A_l^m\langle r^l\rangle$, which are dominated by the lattice contribution, is even better. Richter *et al.* suggest that their non-self-consistent treatment of the non-spherical on-site charge density may be responsible for the 20% difference between their and our values of $A_2^0\langle r^2\rangle$.

Yamaguchi and Asano have performed FLAPW calculations very similar to ours for a number of compounds including $GdCo_5$.[61] Treating the $5p$ states as core (band) states, they obtain values for $A_2^0\langle r^2\rangle$ in $GdCo_5$ of -769 (-707) K compared to our values of -850 (-763) K. Whereas we treat the $4f$ states as core states, Yamaguchi and Asano treat them as band states. This may certainly account for the slightly differing results.

3. B_{EX}

Finally, we come to the exchange field. The energy cost to flip the $4f$ spins is phenomenologically described by the ex-

change Hamiltonian, Eq. (20). The local exchange integrals calculated for $GdCo_5$ by means of Eq. (25) are $I_{s,4f}$, $I_{p,4f}$, and $I_{d,4f}$ are 77, 113, and 85 meV, respectively. Together with the partial magnetic moments $\Delta n_s = 0.049$, $\Delta n_p = 0.078$, and $\Delta n_d = 0.349$ the exchange energy per spin [Eq. (24)] is 21 meV, corresponding to an exchange field of 360 T. The exchange field is seen to be mainly due to the interaction of the $4f$ spins with the $5d$ electrons. The experimental value for $GdCo_5$ as measured with the high-field free-powder method by Liu *et al.* is 240 T.[62] The agreement is only moderate.

Liebs, Hummler, and Fähnle[47] have improved upon the perturbative approach which we have followed by straightforwardly evaluating the change in the total energy when the $4f$ moments are rotated. To do this they performed two self-consistent field calculations; one for the ground-state configuration and another for an excited configuration with the rare-earth $4f$ spins reversed. In this way the conduction-electron spins are allowed to adjust to the reversed exchange field. For $GdCo_5$ they calculate a value for the exchange field of 239 T (Ref. 63) using the LMTO-ASA method with the $4f$ states treated as open core states. A similar result has been obtained by Liu *et al.* using the augmented spherical wave method and treating the $4f$ states as band states. They calculate the exchange field to be 237 T and confirm that there are substantial changes in the conduction-electron moments when the $4f$ spins are reversed.[62]

IV. SUMMARY AND CONCLUSIONS

Using *first-principles* calculations it is shown that an important contribution to the magnetization of YCo_5 is due to orbital moments on the Co atoms. Introducing a dependence of the potential on the orbital moment which increases the calculated orbital magnetic moments and the magnetocrystalline anisotropy energy led to better agreement with experiment without changing the functional dependence of the MAE on the band filling q.

Contrary to the conventional interpretation, the orbital moments on the two types of Co sites are found to be nearly equal. The anisotropy in the total orbital moment as a function of the band filling is found to follow the same trend as the magnetocrystalline anisotropy energy, and is mainly determined by the anisotropy energy in the orbital moment of the Co atoms at the $2c$ sites, as had been proposed as an interpretation of a number of experiments. However, the band-filling dependence is such that for YCo_5 the anisotropy in the orbital moment on the $3g$ site is much larger than that on the $2c$ site. The calculated second-order crystal-field parameter and electric-field gradient are too large in comparison with experiment. Lattice contributions to the potential are shown to be important for a determination of the crystal-field parameter, but not for the EFG. In an analysis of the origin of the magnetocrystalline anisotropy energy, we have found that degenerate energy bands in the neighborhood of the Fermi energy play an important role. A large peak in the density of states is found just below the Fermi level, which has mainly Co $(2c)$ $d_{x^2-y^2}$ and d_{xy} character. Angle-resolved photoemission should be capable of detecting the large magnetization-direction-dependent energy band splittings which we consider to play an important role in determining the observed magnetocrystalline anisotropy. Our calculations of the anisotropy energy as a function of the band filling indicate that anisotropy energies at least twice as large as those found for YCo_5 are, in principle, possible without having to resort to including rare-earth ions. g-factor measurements are necessary to obtain more reliable evidence that a large orbital moment contributes to the magnetic moment. A large scatter in the experimental data for the hyperfine fields prevents a conclusive comparison with our calculated results.

ACKNOWLEDGMENT

We have had numerous discussions with Reinder Coehoorn about various aspects of the work presented here. We are grateful for his drawing our attention to Refs. 62 and 63.

[1] K.H.J. Buschow, A.M. van Diepen, and H.W. de Wijn, Solid State Commun. **15**, 903 (1974).
[2] S.G. Sankar, V.U.S. Rao, E. Segal, W.E. Wallace, W.G.D. Frederick, and H.J. Garrett, Phys. Rev. B **11**, 435 (1975).
[3] R. Radwanski, J. Magn. Magn. Mater. **62**, 120 (1986).
[4] H. R. Kirchmayr and E. Burzo, in *Magnetic Properties of Metals*, edited by H.P.J. Wijn, Landolt-Börnstein, New-Series, Vol. III/19d2 (Springer, Berlin, 1990).
[5] W.G.D. Frederick and M. Hoch, IEEE Trans. Magn. **10**, 733 (1974).
[6] J. Déportes, D. Givord, J. Schweizer, and F. Tasset, IEEE Trans. Magn. **12**, 1000 (1976).
[7] J.M. Alameda, D. Givord, R. Lemaire, and Q. Lu, J. Appl. Phys. **52**, 2079 (1981).
[8] D.M. Paige, B. Szpunar, and B.K. Tanner, J. Magn. Magn. Mater. **44**, 239 (1984).
[9] A.S. Ermolenko, IEEE Trans. Magn. **15**, 1765 (1979).
[10] F. Tasset, Thèse, Université de Grenoble (1975) is the work cited by J. Schweizer and F. Tasset in J. Phys. F **10**, 2799 (1980).
[11] D. Givord, J. Laforest, R. Lemaire, and Q. Lu, J. Magn. Magn. Mater. **31-34**, 191 (1983).
[12] A. Heidemann, D. Richter, and K.H.J. Buschow, Z. Phys. B **22**, 367 (1975).
[13] R.L. Streever, Phys. Rev. B **19**, 2704 (1979).
[14] J. Laforest, R. Lemaire, H. Nagai, and A. Tsujimura, Solid State Commun. **48**, 941 (1983).
[15] H. Yoshie, K. Ogino, H. Nagai, A. Tsujimura, and Y. Nakamura, J. Magn. Magn. Mater. **70**, 303 (1987); H. Yoshie, M. Shiga, and Y. Nakamura, J. Phys. Soc. Jpn. **57**, 1116 (1988).
[16] F.J. van Steenwijk, H.Th. Lefever, R.C. Thiel, and K.H.J. Buschow, Physica **92B**, 52 (1977).
[17] K. Tomala, G. Czjzek, J. Finka, and H. Schmidt, Solid State Commun. **24**, 857 (1977).
[18] P. Hohenberg and W. Kohn, Phys. Rev. **136**, B864 (1964).
[19] W. Kohn and L.J. Sham, Phys. Rev. **140**, A1133 (1965).
[20] U. von Barth and L. Hedin, J. Phys. C **5**, 1629 (1972).

[21] O. Gunnarsson and R.O. Jones, Rev. Mod. Phys. **61**, 689 (1989) and references therein.
[22] G.H.O. Daalderop, P.J. Kelly, and M.F.H. Schuurmans, Phys. Rev. B **41**, 11 919 (1990).
[23] M.S.S. Brooks, Physica **130B**, 6 (1985). A derivation has been given recently by L. Severin, M.S.S. Brooks, and B. Johansson in Phys. Rev. Lett. **71**, 3214 (1993). This modified formulation is not expected to result in any significant changes to the results reported here [M.S.S. Brooks (private communication)].
[24] O. Eriksson, M.S.S. Brooks, and B. Johansson, Phys. Rev. B **41**, 9087 (1990); **41**, 7311 (1990).
[25] O. Eriksson, B. Johansson, R.C. Albers, A.M. Boring, and M.S.S. Brooks, Phys. Rev. B **42**, 2707 (1990). Slightly different, corrected values have been reported by P. Söderlind, O. Eriksson, B. Johansson, R.C. Albers, and A.M. Boring, *ibid.* **45**, 12 911 (1992).
[26] G.H.O. Daalderop, P.J. Kelly, and M.F.H. Schuurmans, Phys. Rev. B **44**, 12 054 (1991).
[27] H. Ebert, P. Strange, and B.L. Gyorffy, J. Phys. F **18**, L135 (1988).
[28] G.H.O. Daalderop, P.J. Kelly, and M.F.H. Schuurmans, J. Magn. Magn. Mater. **104-107**, 737 (1992).
[29] H.J.F. Jansen and A.J. Freeman, Phys. Rev. B **30**, 561 (1984).
[30] O.K. Andersen, Phys. Rev. B **12**, 3060 (1975).
[31] P.E. Blöchl, O. Jepsen, and O.K. Andersen, Phys. Rev. B **49**, 16 223 (1994).
[32] In calculations for Co, and multilayers which contain Co, we found that iterating the Hamiltonian with spin-orbit coupling included did not lead to different results.
[33] G.H.O. Daalderop, P.J. Kelly, and M.F.H. Schuurmans, Phys. Rev. B **50**, 9989 (1994).
[34] B.R. Judd, *Operator Techniques in Atomic Spectroscopy* (McGraw-Hill, New York, 1963).
[35] G.H.O. Daalderop (unpublished).
[36] E. Fermi, Z. Phys. **60**, 320 (1930).
[37] H. Ebert, J. Phys. Condens. Matter **1**, 9111 (1989).
[38] S. Blügel, Akai, R. Zeller, and P.H. Dederichs, Phys. Rev. B **35**, 3271 (1987).
[39] G.H. Dieke, *Spectra and Energy Levels of Rare Earth ions in Crystals* (Wiley, New York, 1968).
[40] M.T. Hutchings, *Solid State Physics: Advances in Research and Applications*, edited by F. Seitz and D. Turnbull (Academic, New York, 1964), Vol. 16, p. 227.
[41] V. Heine, *Group Theory in Quantum Mechanics* (Pergamon, Oxford, 1960).
[42] K.W.H. Stevens, Proc. Phys. Soc. London Ser. A **65**, 209 (1952).
[43] M. Weinert, J. Math. Phys. **22**, 2433 (1981).
[44] P. Blaha, K. Schwarz, and P.H. Dederichs, Phys. Rev. B **37**, 2792 (1988).
[45] M.S.S. Brooks and B. Johansson, J. Phys. F **13**, L197 (1983).
[46] M.S.S. Brooks, L. Nordström, and B. Johansson, J. Phys. Condens. Matter **3**, 2357 (1991); **3**, 3393 (1991).
[47] M. Liebs, K. Hummler, and M. Fähnle, J. Magn. Magn. Mater. **124**, 239 (1993).
[48] O.K. Andersen and O. Jepsen, Phys. Rev. Lett. **53**, 2571 (1984).
[49] This value differs slightly from the values reported by Eriksson *et al.* in Ref. 25. For bcc Fe, hcp Co and fcc Ni we calculate orbital moments of 0.077, 0.129, and 0.076 μ_B, respectively, compared to values of 0.06, 0.14, and $0.07\mu_B$ reported by Eriksson *et al.* and 0.09, 0.14, and $0.07\mu_B$ reported by Söderlind *et al.* Our orbital polarization calculations were carried out with an *s,p,d,f* basis and with 165, 196, and 196 inequivalent **k** points, respectively. The corresponding spin moments were 2.144, 1.573, and $0.604\mu_B$.
[50] S.K. Malik, F.J. Arlinghaus, and W.E. Wallace, Phys. Rev. B **16**, 1242 (1977).
[51] B. Szpunar and V.H. Smith, J. Solid State Chem. **88**, 217 (1990).
[52] L. Nordström, O. Eriksson, M.S.S. Brooks, and B. Johansson, Phys. Rev. B **41**, 9111 (1990).
[53] L. Nordström, M.S.S. Brooks, and B. Johansson, J. Phys. Condens. Matter **4**, 3261 (1992).
[54] When determining the magnetocrystalline anisotropy energy using the Sucksmith-Thompson method, account must be taken of the anisotropy of the magnetic moment. Energies of about 5 meV/unit cell result when this is neglected (Refs. 5 and 6), otherwise an energy of about 3.8 meV/unit cell is found (Ref. 7).
[55] J. Friedel, in *The Physics of Metals*, edited by J.M. Ziman (Cambridge University Press, Cambridge, 1969). Earlier on we argued that the most important contribution to the *c*-axis orientation came from the splitting of a doubly degenerate state. The energy gain from such a splitting is $\sim\xi$ and is not consistent with the observed quadrupling of the anisotropy energy when the spin-orbit coupling parameter is effectively doubled. The reason for this apparent contradiction is that the number of electrons whose energy is lowered by the spin-orbit interaction increases when the spin-orbit coupling parameter increases. The actual dependence of the anisotropy energy on ξ depends on the band dispersion.
[56] P. Bruno, Phys. Rev. B **39**, 865 (1989).
[57] R. Coehoorn, K.H.J. Buschow, M.W. Dirken, and R.C. Thiel, Phys. Rev. B **42**, 4645 (1990).
[58] P. Blaha, K. Schwarz, and P. Herzig, Phys. Rev. Lett. **54**, 1192 (1985).
[59] R. Coehoorn and K.H.J. Buschow, J. Appl. Phys. **69**, 5590 (1991); K.H.J. Buschow, R. Coehoorn, F.M. Mulder, and R.C. Thiel, J. Magn. Magn. Mater. **118**, 347 (1993).
[60] M. Richter, P.M. Oppeneer, H. Eschrig, and B. Johansson, Phys. Rev. B **46**, 13 919 (1992)
[61] M. Yamaguchi and S. Asano, J. Phys. Soc. Jpn. **63**, 1071 (1994).
[62] J.P. Liu, F.R. de Boer, P.F. de Chatel, R. Coehoorn, and K.H.J. Buschow, J. Magn. Magn. Mater. **132**, 159 (1994).
[63] T. Beuerle, M. Liebs, K. Hummler, and M. Fähnle, J. Magn. Magn. Mater. **132**, L1 (1994).